Surface Characterization of Titanium Powders with X-ray Photoelectron Spectroscopy

by

SARA AXELSSON

Diploma work No. 103/2012
at Department of Material and Manufacturing Technology
CHALMERS UNIVERSITY OF TECHNOLOGY
Gothenburg, Sweden

Diploma work in the Master Programme Advanced Engineering Materials

Performed at: Department of Materials and Manufacturing Technology
SE-412 96 Gothenburg

Supervisors: Dr. Ulf Ackelid
Arcam AB
Krokslätts Fabriker 27A
SE-437 37 Mölndal

Dr. Yu Cao
Department of Materials and Manufacturing Technology
SE-412 96 Gothenburg

Examiner: Prof. Uta Klement
Department of Materials and Manufacturing Technology
SE-412 96 Gothenburg

Surface Characterization of Titanium Powders with X-ray Photoelectron Spectroscopy
SARA AXELSSON

Diploma work no. 103/2012
Department of Material and Manufacturing Technology
Chalmers University of Technology
SE-412 96 Gothenburg
Sweden
Telephone +46(0)31-772 1000

Cover:
SEM image of a Ti-6Al-4V powder particle

Reproservice
Gothenburg, Sweden 2012

Surface Characterization of Titanium Powders with
X-ray Photoelectron Spectroscopy
SARA AXELSSON
Department of Materials and Manufacturing Technology
Chalmers University of Technology

Abstract

Electron Beam Melting (EBM®) is a near-net-shape additive manufacturing technology developed by Arcam AB, where Ti-6Al-4V alloy powder is commonly used to manufacture medical implants and components for the aerospace industry. Although Arcam has developed special specifications of some parameters for the powders, the powders from different manufacturers do not behave in the same way in the EBM process. Differences also have been detected for powder that have been reused in the process. It is believed that the variations in the behaviour in the process arise due to differences in the native oxide surface layer of the powder particles.

Therefore, the aim of this project was to characterize the surface oxides on Ti-6Al-4V powders in order to compare powders from different manufacturers, new and recycled powders as well as powder before and after an anti-satellite treatment made to reduce small particles (satellites) on the powder surfaces. X-ray photoelectron spectroscopy (XPS) and scanning electron microscopy (SEM) were used to obtain information about the chemical composition, the in-depth distributions, the chemical states of the elements in the surface oxide, the oxide thickness, as well as the shape and the morphology of the powder particles.

The results showed that the surface oxide contained titanium mostly in the form of TiO_2 and aluminium in the form of Al_2O_3 in all samples. The vanadium was impoverished at the powder surface whereas the aluminium content was enriched. Yttrium was also found on the powder surfaces from one manufacturer. The investigation of the new and recycled particles showed that the vanadium content was higher on the outermost surface. Furthermore, the powder surface was rougher, and, after several cycles of recycling, the surface oxide was thicker. The anti-satellite treatment did not affect the chemical composition, the chemical state or the oxide thickness.

Keywords: Ti-6Al-4V, surface oxide, XPS, powder, Electron Beam Melting

Acknowledgement

First, I would like to thank my supervisor Ulf Ackelid at Arcam AB for his great support and enthusiasm during my work.

To my supervisor at Chalmers Yu Cao, I would like to say thank you for answering all my questions and for all help. Thank you also to my examiner Uta Klement. Furthermore, I would like to thank everyone at the Department of Materials and Manufacturing Technology who helped me during my work.

Finally, I would like to give a special thanks to my family and friends for supporting and believing in me.

Göteborg, October 2012
Sara Axelsson

Contents

Chapter 1

Introduction

1.1 Background

Titanium and its alloys are very useful materials due to their high strength-to-weight ratio. However, the drawback of titanium is the high price due to the complicated production process. In order to reduce material waste, it is therefore preferable to use a near-net-shape technology such as additive manufacturing.

Electron Beam Melting (EBM®) is an additive manufacturing process developed by Arcam AB. Three-dimensional components are built up from a CAD-model by selectively melting and densifying each layer of powder with an electron beam. The titanium alloy Ti-6Al-4V is a material commonly used in the EBM process to manufacture medical implants and components for the aerospace industry.

For the metal powder used in this process, Arcam has developed special specifications of some parameters for the powder manufacturers, such as particle size distribution, chemical composition etc. Although the specifications are fulfilled, powders from different manufacturers do not behave in the same way in the EBM process with respect to sinterability and sensitivity to charge build-up when exposed to the electron beam. Differences in behaviour have also been detected between new powder and powder that has been reused in the process.

It is believed that the variations arise due to differences in the native oxide surface layer of the powder particles. The volume of the surface layer is too small to influence the average chemical composition of the whole particle; however, it is still very influential for the electrical and thermal behaviour of the powder.

1.2 Aim

The aim of this study is to characterize the surface oxides on different Ti-6Al-4V powders. The powder samples are selected to enable comparisons between:

- new powders from three different manufacturers
- powder before and after it has been recycled in the EBM process
- powder before and after a so-called anti-satellite treatment, made in order to reduce the amount of small particles (satellites) attached to the powder surfaces

The information that will be analysed for the powder samples is

- the chemical composition
- the in-depth distribution of the elements
- the chemical states of the elements
- the oxide thickness
- the shape and morphology of the powder particles

1.3 Method

First, a literature study will be performed to gather information and study previous work on the subject. For surface characterization, X-ray photoelectron spectroscopy (XPS) will be used to investigate the chemical compositions and the chemical states. By ion etching with Ar^+-ions, depth profiles will be obtained to examine the change in composition with depth. Furthermore, the surface oxide thickness will also be estimated. The powders will also be examined in a scanning electron microscope (SEM) to investigate the shape and morphology of the powder particles.

Chapter 2

Titanium and titanium alloys

The main advantage of titanium is its high strength-to-weight ratio. Its strength is comparable to steel, but the density is just the half of it. It also possesses good mechanical properties and corrosion resistance, which is maintained even at higher temperatures [1]. Because of these properties, titanium is mainly used in areas where corrosion resistance or lightweight is needed [2], such as airframe components and jet engines in the aerospace industry, in the pulp and paper industry, in marine applications, in the automotive industry, for sports equipment [3], for heat exchangers, for chemical and food processing as well as for biomedical applications such as implants [4].

2.1 Production technology

Titanium is the ninth most abundant material in the Earth's crust, but the problem is that it is never found in high concentrations or in its pure state, making it hard and costly to process. It is usually found as ilmenite, $FeTiO_3$, or rutile, TiO_2, in mineral sands [5]. In order to process titanium, the extended Kroll process is used where the ilmenite or rutile is transformed into titanium tetrachloride and finally reduced by magnesium [6].

Titanium can be manufactured in many ways, for example: forging, welding, casting or by means of powder metallurgy [1]. Because of the high price of titanium, near-net-shape techniques, such as additive manufacturing, are commonly used to reduce manufacturing steps and material waste [7].

2.2 Structure

Titanium has a transformation temperature of 882°C, at which it undergoes an allotropic transformation [2]. Below this temperature, it has a hexagonal

closed-packed crystal structure (HCP) called the α phase; above this temperature, it has a body-centred cubic structure (BCC) referred to as the β phase. These phases are shown as a) and b) respectively in Figure 2.1. The fact that titanium has two crystal structures makes is possible to tailor the properties of the titanium alloys [5].

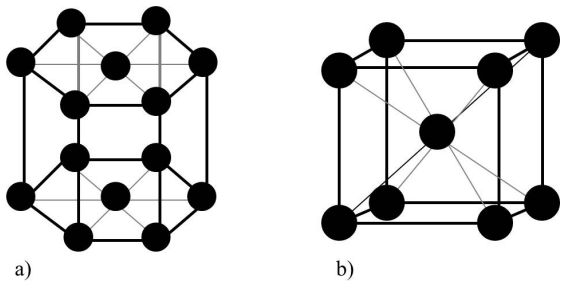

Figure 2.1: The crystal structures of titanium, a) HCP and b) BCC. Adapted from [5].

The effect of the alloying elements may be neutral, α or β stabilising [2]. The α stabilizers raise the α-β transformation temperature in order to stabilize the α phase, while the β stabilizers lower the transition temperature and make the β phase stable at room temperature [8].

Depending on the heat treatment, different microstructures can be obtained, which can be described by the arrangement and size of the α and β phases. The lamellar structure is formed when the material is cooled slowly from the β phase region. During this cooling the α phase grows as lamellae into the β grains. Depending on the cooling rate, the lamellae may be fine or coarse. A considerably faster cooling method, quenching, leads to a martensitic microstructure with fine needles. However, unlike steel, the martensitic hardening is just moderate for titanium. Equiaxed microstructure is obtained by recrystallization after cold working. The microstructure can be coarse or fine depending on the solution annealing time. The biomodal, or duplex, microstructure is a combination of lamellar and equiaxed structures [5]. The Widmanstätten microstructure consists of parallel plates of α phase with β phase in-between [1]. The microstructure thus has a large influence on the properties of titanium alloys.

2.3 Properties

The melting point of titanium is 1660°C and its density is 4.51 g/cm^3. The conventional titanium alloys have a yield strength in the range of 800-1200 MPa and a Young's modulus of around 100-140 GPa. Titanium alloys maintain strength only up to temperatures around 500°C due to their oxidation behaviour [5]. At elevated temperatures, thick oxide is formed and

this reduces the cross-section that bears the load [9]. However, titanium aluminides, TiAl, have better oxidation behaviour and can be used at temperatures up to 800°C [5]. Other properties are a low thermal expansion coefficient, essentially non-magnetic and excellent cryogenic properties [10].

Titanium and its alloys possess all important properties for medical applications such as corrosion resistance, biocompatibility, bioadhesion, suitable mechanical properties and processability [11]. Commercially pure titanium or the Ti-6Al-4V alloy are mostly used and the applications are, for example, hip implants, knee implants, bone staples and dental implants [12]. Other materials in addition to titanium that are used for these applications are stainless steels, cobalt-chrome alloys and tantalum [11], [12]. The corrosion resistance is of major importance in order to avoid spreading of the metal ions and damage of the body as well as the function losses of the implant [11]. On titanium, a stable, dense, non-conductive oxide film is formed, which prevents the flow of ions making it biocompatable [11], [13]. The advantage of titanium and its alloys for load bearing orthopaedic implants is its low Young's modulus [12]. Its value is the closest to the Young's modulus of the bone among all metallic biomaterials, which gives better transfer of the load and, thus, stimulates the bone growth [11]. Furthermore, direct bonding of the bone tissue to the implant material has only been detected for titanium [12]. However, the drawback of titanium for this applications is its low hardness, which leads to low wear resistance and low shear strength, making it less suitable for applications such as bone screws and plates [12], [14].

The properties of titanium may be improved by alloying and/or processing. Alloying elements harden the material by precipitation and solid solution. Moreover, density, corrosion and oxidation behaviour can also be changed [5]. The alloying elements will be discussed further in section 2.4. By processing, the microstructure and the grain size can be tailored [5]. Generally, fine structures give higher strength, higher ductility and better fracture toughness, while the coarse structure is more resistant to creep and fatigue [5], [15]. Ductility and fatigue strength are also higher for an equiaxed microstructure while a lamellar structure has increased fracture toughness and resistance to creep and fatigue.

2.4 Titanium alloys

There are many titanium alloys with different chemical compositions and microstructures, and these possess a wide range of properties. The transformation temperature between the α and β phase is influenced by interstitial oxygen, nitrogen and carbon, which stabilizes the α phase, hydrogen, which acts as a β stabilizer, and metallic alloying elements with varying effects [1]. Typical alloying elements that act as α stabilizers are aluminium, carbon,

gallium, germanium and nitrogen [1], [9], whereas vanadium, niobium and molybdenum are β stabilizers [3]. Aluminium is the principal α stabilizer, although a content of over 6 wt% exceeds the solid solution limit and forms brittle intermetallic Ti_3Al [8]. Other common alloying elements are tin and zirconium, which strengthen both the α and the β phase by solid solution [1]. Niobium is added to improve oxidation resistance at high temperatures and molybdenum gives better hardenability and short-time elevated temperature strength [8]. The main categories of titanium alloy are α alloys, near-α alloys, α+β alloys and metastable β alloys.

The α alloys have excellent properties at high temperature [3]. The HCP structure in the α phase has fewer slip systems than the BCC structure, leading to limited plastic deformation and lower ductility [5]. The highly packed structure also gives a low diffusion coefficient, making it more resistant to creep and oxidation [5]. Furthermore, the α alloys have very high resistance to corrosion [5] and good weldability, but they cannot be strengthened by heat treatments [3]. Pure titanium often contains a small amount of interstitial oxygen, which increases its strength [1]. The different grades of unalloyed titanium depend on the oxygen and iron content [1]. The main application areas for these alloys are in the chemical and process engineering industry, where corrosion and deformability are the main properties required [5].

The near-α alloys contain both α and a small amount of β stabilizing elements [1], [8]; examples of such alloys are Ti-8Al-1Mo-1V and Ti-6Al-2Nb-1Ta-0.8Mo [1]. The microstructure contains a small amount of retained β phase. These alloys combine the excellent creep behaviour of the α alloys with the high strength of α+β alloys [5]. This makes near-α alloys perfect for high temperature service up to a temperature of 500 to 550°C [5]. These alloys are, for example, used in gas turbine engines, aircraft engine compressor blades as well as airframe and jet-engine parts [5].

The α+β alloys are the far most popular, used, tested and developed titanium alloys as they have a good balance between the desired properties. The most common titanium alloy, Ti-6Al-4V, is of this type and accounts for more than half of the titanium alloys used today [5]; this alloy is described in more detail in Section 2.4.1.

Metastable β alloys have the highest strength of all titanium alloys [5]. The properties of these alloys also include high toughness, high fatigue strength, excellent forgeability and the ability to be strengthened by heat treatment [1], [16]. However, the high strength may lead to low ductility [5]. Other disadvantages are higher density, modest weldability and poor oxidation behaviour [5]. One example of a β alloy is the Ti-10V-2Fe-3Al [1]. The applications for the metastable β alloys are rotor heads for helicopters and air plane landing gears [16].

2.4.1 Ti-6Al-4V

The most common and widely used titanium alloy is Ti-6Al-4V, an $\alpha + \beta$ alloy [17]. As the name says, it contains around 6 wt% aluminium and 4 wt% vanadium. The vanadium content is higher than the solubility of vanadium in the α phase, making an amount of the β phase stable at room temperature [18]. The β phase has a higher content of vanadium than the α phase [19].

This alloy has been developed for aerospace applications to improve the mechanical properties of titanium while keeping the corrosion resistance intact [19]. To show its advantages, a comparison of the mechanical properties of Ti-6Al-4V and commercially pure titanium (Grade 2) can be seen in Table 2.1.

Table 2.1: Comparison of mechanical properties of Ti and Ti-6Al-4V at room temperature [8]

Property	Ti	Ti-6Al-4V
Ultimate tensile strength (MPa)	240-330	900-990
Yield strength (MPa)	170-240	830-920
Elongation (%)	30	14
Reduction in area (%)	55	30

Furthermore, Ti-6Al-4V has good workability [20]. The alloy is heat treatable, which makes it possible to tailor its properties [18]. The tribological properties (interaction of surfaces such as friction, wear and lubrication) are better for Ti-6Al-4V than for pure titanium [4]. The Ti-6Al-4V ELI (extra low interstitial) is an alloy with less oxygen and iron and has been developed to increase the toughness [1].

The alloy is used in many different areas, for example, aerospace applications, pressure vessels, aircraft turbine and compressor blades and surgical implants [1].

There are several standards for the chemical composition of Ti-6Al-4V; these are used for different purposes. Three of them are i) ASTM F136 Standard Specification for Wrought Ti-6Al-4V ELI (extra low interstitial) alloy for surgical implant applications [21], ii) ASTM F1472 Standard specification for wrought Ti-6A-4V alloy for surgical implant applications [22] and, iii) ISO 5832-3 implants for surgery-metallic materials Wrought Ti-6A-4V alloy [23]. The compositions of these standards are listed in Table 2.2.

Table 2.2: Chemical composition of Ti-6Al-4V in wt %

Element	ASTM F1472	ASTM F136	ISO 5832
Al	5.5-6.75	5.5-6.5	5.5-6.75
V	3.5-4.5	3.5-4.5	3.5-4.5
Fe	<0.3	<0.25	<0.3
O	<0.2	<0.13	<0.2
N	<0.05	<0.05	<0.05
H	<0.015	<0.012	<0.015
C	<0.08	<0.08	<0.08
Y	<0.005	-	-
Ti	bal.	bal.	bal.

2.5 Titanium oxides

Titanium is a transition metal with a partly filled d-band; it and has several available chemical states and may form very stable oxide films. The most common oxidation state of titanium is Ti^{4+} (TiO_2), but the lower states Ti^{3+} (Ti_2O_3) and Ti^{2+} (TiO) also occur [19]. Titanium has a very high affinity to oxygen; only a very low oxygen pressure is needed to oxidise titanium fully to TiO_2 [24]. Titanium dioxide is a thermodynamically very stable compound; it may exist as three different crystalline structures: anatase (tetragonal), rutile (tetragonal) and brookite (orthorhombic) [19].

Rutile is used in the production of titanium and for melding-rod coatings. Titanium oxide is mostly used as white pigments in paints, varnishes and lacquers because of its high opacity and chemical inertness [25]. Other applications are as photocatalysts, in solar cells for production of hydrogen and electric energy, in ceramics and in corrosion-protective coatings [26].

2.5.1 Surface oxides on titanium and its alloys

When a metal surface is exposed to air, it will interact with it. Titanium is very reactive and an oxide layer may easily form on the surface [19]. It has a high affinity for oxygen; moreover, oxygen has a high solubility in titanium [2]. Figure 2.2 shows how the surface oxide is formed. First, the oxygen forms a monolayer on the surface. The oxide is then formed by diffusion of the oxygen atoms into the material and/or metal ion diffusion onto the surface [19]. After the nucleation, the oxide grows laterally to cover the whole surface [9]. Then the oxide film grows in thickness, and the diffusion rate of the atoms and ions will decrease until it becomes zero and the growth stops [19]. The surface oxide layer will now protect the surface from further oxidation. If the oxide film is damaged, it may, with only a small amount of oxygen or water present in the environment, spontaneously self-heal [27].

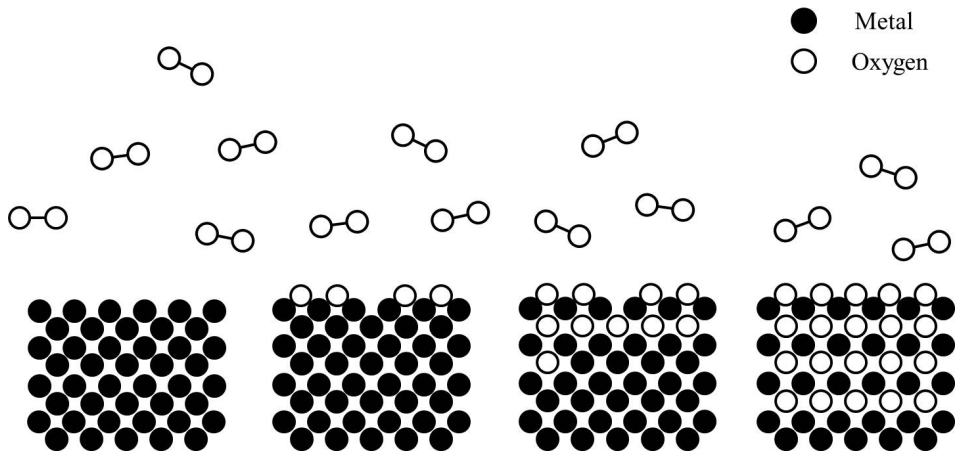

Figure 2.2: Formation of oxide on a metal surface. Adapted from [28]

Several studies have been conducted on the surface oxide of titanium and its alloys in different conditions: sterilized [29], [30], [31]; machined [29]; cleaned [29]; electropolished [29]; anodic oxidized [4], [29]; thermal oxidized/heat treatment [4], [29], [32]. Commonly used methods for these studies are surface-sensitive techniques such as X-ray photoelectron spectroscopy (XPS), Auger electron spectroscopy (AES) and secondary ion mass spectroscopy (SIMS). However, fairly few studies have been conducted on native air-formed oxide films.

Crystal structure of titanium surface oxides

The nature and thickness of the surface oxide depends on the environmental conditions. Oxide layers spontaneously formed on titanium in air have a thickness of about 5-10 nm [30], [33]. In previous work, it has been found that the crystal structure of the surface oxide formed naturally may be either anatase TiO_2 [32] or rutile [2]. High temperature oxidation, above 800°C, often leads to a TiO_2 rutile crystal structure, which is more stable and more dense [27], [34]. In contrast, a lower temperature gives an amorphous structure or a mixture of the two structures [27].

Composition and oxidation states

Lausmaa [29] conducted a study on the surface of commercially pure titanium that was machined, cleaned in organic solvents and then sterilized. The XPS-survey spectrum showed strong signals of titanium, oxygen and carbon and less intensive peaks from calcium, potassium, silicon, sodium, chlorine, nitrogen and sulphur. After a few nm of sputtering, all signals except from the titanium and oxygen had disappeared, indicating that the

other elements were contamination on the surface. TiO_2 and metallic titanium could easily be distinguished in the XPS spectrum, but there were also small contributions between these two peaks, these could be TiO, Ti_2O_3, titanium hydroxide, titanium nitride and/or titanium carbide. On machined surfaces, carbides and nitrides can often be detected. The nitrogen peak may come from both organic molecules and nitrides, TiN_x.

Carley et al. [35] detected sub-oxides on room-temperature oxidized titanium foil with oxide films thinner than the penetration depth of the XPS. The thick oxide layers formed at high temperature showed only TiO_2 on the unsputtered surface. Angle resolved XPS (ARXPS) showed that the native oxides TiO and Ti_2O_3 are most probably located at the metal-oxide interface.

Surface oxides on the Ti-6Al-4V alloy

The oxidation of alloys may be different from the oxidation of pure metals. Some of the factors that influence the oxidation of an alloy are the alloy composition, the base material, the diffusion within the alloy, the ratio of the rate of formation of different oxides, and the enthalpy of formation of the oxides [9]. This may give an oxide with a different composition than the base material and also a different morphology than the oxide on a pure metal.

To be able to protect the underlying metal, the oxide has to meet some requirements such as good adhesion to the metal, a good crack healing ability, high thermodynamic stability in the working environment and low vapor pressure of the oxide [9]. Al_2O_3 is one of the oxides that fulfill these requirements best [9]. The surface oxides on some alloys containing aluminium consist only of Al_2O_3. However, in the case of titanium alloys, the TiO_2 is equally stable and thus inhibits the growth of aluminium oxide, wherefore the oxide consists of both titanium and aluminium [9]. In surface oxides on Ti-6Al-4V formed naturally in air, the aluminium has been detected as Al_2O_3 and is enriched at the surface [29], [36].

Vanadium cannot be detected at the outermost surface in natural oxides; it is located below the top surface and may only be observed after some sputtering either by XPS or AES [19], [31], [37]. The vanadium seems to be mainly in the state of V_2O_5, with contributions of V_2O_3 and VO_2 [36]. The alloy has an $\alpha+\beta$ structure where the β-phase has a higher vanadium content, leading to a lateral variation of the vanadium also in the oxide. This has been confirmed with AES by Hernández de Catica et al. [31]. V and Al could also be present as interstitial or substitutional ions in the titanium oxide matrix [36].

Lee et al. [38] conducted an XPS study on spherical atomized Ti-6Al-4V powder with the diameter of 150-200 μm, both in as-received and argon ion etched conditions. The main elements before sputtering were carbon, oxygen

and titanium, but there were also small peaks from aluminium, vanadium and nitrogen. The titanium was mainly in form the of TiO_2; after sputtering, metallic titanium was also detected. The aluminium in the oxide was present as Al_2O_3. The nitrogen was present in organic form and as nitride, though after some sputtering, the organic contribution could no longer be seen.

Reduction of titanium oxide during sputtering

A study of native air-formed oxide film on 99.99% titanium foil by McCafferty et al. [33] using ARXPS showed that the surface consisted only of TiO_2. When the sample was sputtered, the sub-oxides were detected after just 30 seconds (1.5 Å). If the sub-oxides had been at this depth from the beginning, they would have been detected by the ARXPS. This showed that the sub-oxides Ti_2O_3 and TiO just came from the ion beam reduction of TiO_2. It seems that the ion beam reduces the TiO_2 to Ti_2O_3, which is further reduced to TiOm, due to the fact that TiO increases and TiO_2 decreases while Ti_2O_3 is quite stable over sputtering time.

Idriss et al. [39] also showed that the Ar^+-ion sputtering may change the chemical states and composition. A single crystal of TiO_2 was sputtered with Ar^+-ions and afterwards, Ti^{1+}, Ti^{2+}, Ti^{3+} and Ti^{4+} were detected by XPS. However, no Ti^0 metal was detected, which indicates that no oxide is reduced to metal by the ion bombardment.

Chapter 3

Additive manufacturing of titanium components by Electron Beam Melting

Additive manufacturing is the general term for all manufacturing techniques where the component is built by adding material layer by layer. In contrast to the more common and long-used subtractive manufacturing technique machining, where material is removed from the raw material block. These techniques are sometimes called 3D-printing or rapid prototyping, because they were first developed to make prototypes to speed up the product development [40]. With additive manufacturing, a complex 3D component can be made directly from a CAD-model. The model is then sliced into 2D layers with a determined thickness. At the manufacturing, the layers of liquid, powder or sheet material are added together to form a component [41]. The technique was first developed for polymers, but is now used for all types of materials including metal, ceramics and composites [40]. There are many different additive manufacturing techniques available such as laser beam melting, electron beam melting, selective laser sintering, fused deposit modelling and laminated object manufacturing [40].

The advantage of additive manufacturing are that the components may be produced faster with fewer manufacturing steps; this enables faster product development and a more efficient use of the material [40]. Furthermore, it is possible to produce components that are too complex to produce by traditional techniques [42]. However, the disadvantages are that the machines need careful maintenance, the raw material is more expensive and may need careful handling [40]. Moreover, these techniques have relatively low productivity [42].

3.1 Electron Beam Melting, EBM®

Electron Beam Metling, EBM®, is an additive manufacturing process developed by the Swedish company Arcam AB. The process makes it possible to produce fully dense near-net-shape 3D components, which are almost impossible, or at least very complex, to produce with other fabrication techniques [43]. The materials commonly used in the process are unalloyed commercially pure titanium, the titanium alloy Ti-6Al-4V and cobalt-chrome [44]. The applications for the components are expanding constantly with the development of the technology. Currently, the most common applications for the components are medical implants and functional parts for aerospace applications [44]. The maximum size of components built by Arcam A2 machine is 200×200 mm and a height of 350 mm or a circular cross section with a diameter of 300 mm and a height of 200 mm [45].

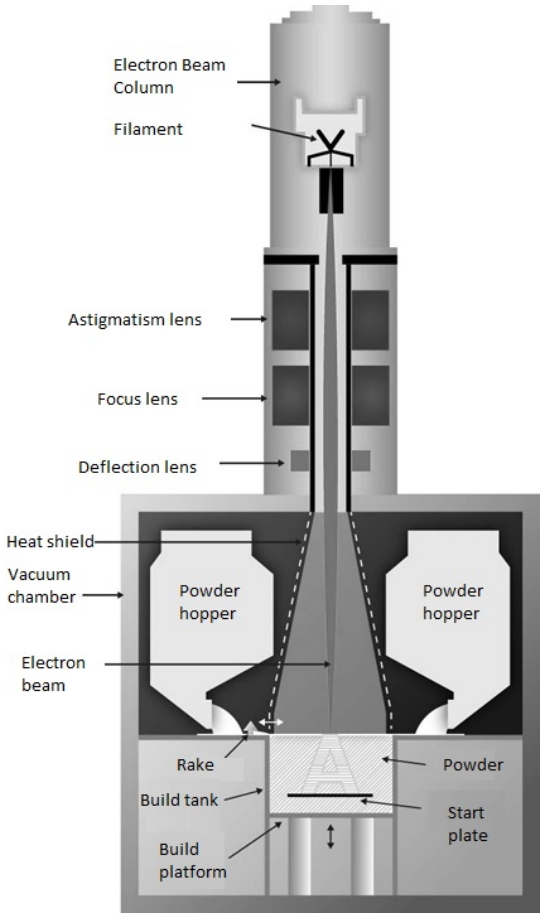

Figure 3.1: Schematic picture of an EBM machine. [Published by courtesy of Arcam AB]

In this process, an electron beam is used to sinter and melt the metal powder [43]. A schematic picture of the machine and its components can be seen in Figure 3.1. In the electron beam gun, a tungsten filament is heated in order to emit electrons. The electrons are then collimated and accelerated to an energy of 60 keV. The electrons pass through three magnetic lenses: one to correct for the astigmatism of the beam, one to focus the beam down to 0.1 mm, and the last one to deflect the beam to make it sweep over the building table. The current of the beam in the machines is today between 1 and 50 mA.

First, a 3D CAD-model of the component to be produced is made. Then the model is cut into slices with the layer thickness of the powder, usually 0.05 to 0.1 mm [43]. A layer of powder from the powder hopper is raked onto the start plate and the beam sweeps over the powder and heats the first layer. Figure 3.2 shows an example of how the different layers in a component are melted. The powder is first preheated to a temperature of approximately 80% of the melting temperature of the material [46] to sinter the powder lightly to fix it in order to avoid it from spreading [47]. Then the beam is scanned at slower speed over selected parts of the powder bed in order to melt the powder. The build platform is lowered, new powder is raked out and the building of the second layer starts. During the whole build time, the component is kept at an elevated temperature. For Ti-6Al-4V it is approximately 600-700°C [42]. The building speed is typically 3-6 mm per hour [43]. The building time is dependent on the size of the component but usually 10 to 100 hours [42].

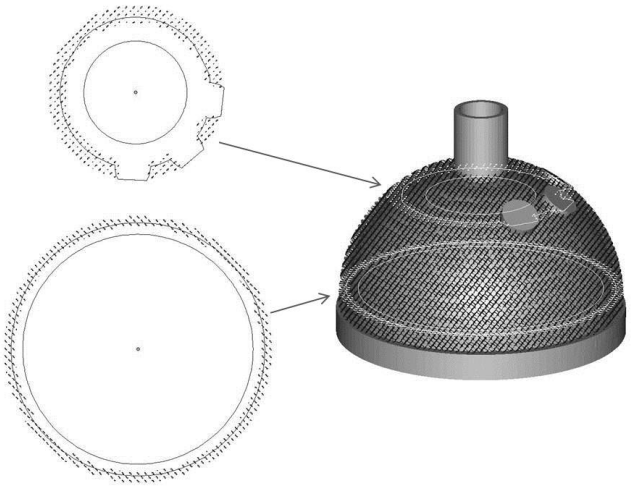

Figure 3.2: The figure shows two different layers and their positions in the sliced 3D model of the final component, an acetabular cup. The cross-sections show the areas that are selectively melted in the EBM process. [Published by courtesy of Arcam AB]

The whole process is performed in high vacuum; the base pressure is 10^{-3} Pa in the building chamber and 10^{-5} Pa in the electron gun. The vacuum is necessary partly to avoid collisions between the electrons emitted from the gun and the residual gas molecules, which might scatter the electrons. Furthermore, the clean environment for the molten metals reduces contamination and oxidation [43].

When the building of the component is completed, it is cooled down in the chamber with the help of helium gas at 400 mbar to a temperature of 100°C and then cooled in air [42]. When the component is taken out from the chamber, it is covered by lightly sintered and agglomerated powder, which is blasted away later on [17]. The residual powder from the process is sieved and mixed with non-sintered powder in order to obtain a homogeneous blend [42]. All the loose powder is later reused in the process [43]. In Figure 3.3, two examples of components built by EBM are shown.

Figure 3.3: An acetabular cup for a hip replacement and a turbine blade produced by EBM. [Published by courtesy of Arcam AB]

The heat treatment of the material is inherent in the EBM process. The general microstructure for Ti-6-Al-4V consists of fine elongated epitaxial grown β grains, with acicular or plate like α phase with a Widmanstätten structure, grown from former β boundaries [43].

Compared to the similar laser beam melting process, this process is faster due to the deeper penetration and higher power of the electron beam [42] and the parts are more dense [47]. The drawback is the relatively rough surface [47].

The fact that components are made only as CAD-models, without moulds being used, makes it easy to produce customer-designed parts for medical

and dental implants [47]. The porous structure that can be built in the EBM machine is very favourable for biomaterials. Porosity lowers the elastic modulus of the material making it closer to the elastic modulus of bone, thus avoiding a mismatch [48]. Furthermore, the implant is lighter and the tissue integration better. These facts together with the biocompatibility make titanium alloy manufactured by EBM a good choice for medical implants.

3.2 Powder production

There are several commercial ways of producing metal powders including chemical, electrolytical and mechanical methods as well as atomization. Atomization is the most common process [49] due to the high production rate [50]. Furthermore, in this process, it is often possible to control size, size distribution, shape and surface morphology of the powder [49]. The basics of atomization is to melt metal and break up the liquid into spherical droplets solidifying into powder [50]. The break up can be done in different ways: by introducing water or gas (two-fluid atomization), by the centrifugal force or by mixing the liquid metal with a gas and transferring it from high pressure to vacuum [49]. The ideal powder for additive manufacturing is completely spherical, because of its good flow characteristics and high packing-density [42].

3.2.1 Gas Atomization

In gas atomization, the metal is melted and then subjected to a high-velocity gas that breaks it into droplets. The gas is usually air, nitrogen, argon or helium [50]. In order to make titanium powder, an inert gas is used instead of air because of the high reactivity of titanium with oxygen [49]. The mechanism of the formation of droplets may be divided into three steps. First, a sinusoidal wave is formed, then the wave is fragmented and formed into ligaments and finally it breaks down into droplets [50], as shown in Figure 3.4.

There are three different designs of gas-atomizing units; internal mixing and two different designs of nozzles: free-fall or confined ones [50]. In the free fall process, the liquid metal falls down freely while subjected to the gas stream, though the efficiency of the stream leads to larger particles compared with the confined nozzle. The confined nozzle is designed to maximize the gas velocity and density in contact with the metal. The problem with this type of nozzle is that the powder may solidify in the nozzle opening and block it. In the internal mixing design, the molten metal is mixed with gas under high pressure and then led into an atomization chamber at lower pressure. The difference in pressure makes the metal expand and form droplets.

The gas pressure for conventional atomization is 0.5 to 4 MPa [50]. The velocity of the gas in the confined nozzles is approximately Mach 1 to 3

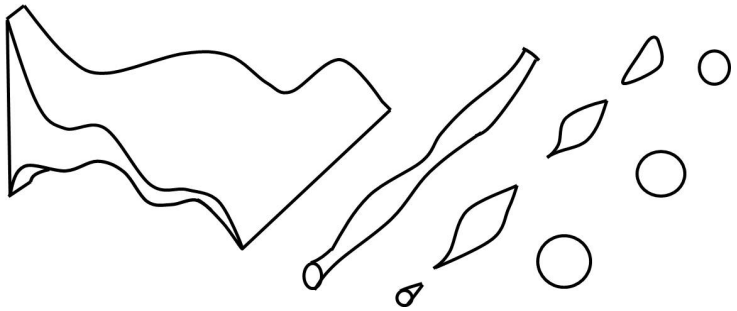

Figure 3.4: Model for formation of droplets in gas atomization. Adapted from [50].

and for free-fall atomizers the velocity is 50-150 m/s when the gas reaches the melt. The average particle size of the powder produced is in the range of 10 to 300 μm, depending on the ratio between metal and gas pressure. An increased gas flow leads to smaller particles. The powder is typically spherical and has a log-normal size distribution.

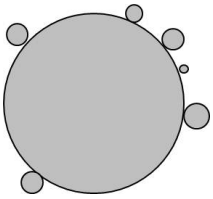

Figure 3.5: Powder particle with satellites

One drawback with the gas atomization process is that gas may be captured in the particles when droplets collide during the solidification [50]. Later, when the powder is sintered, this leads to a microporosity in the final product. Another drawback is that, on the spherical particles, satellites may be detected as smaller spheres attached to the surface of the powder particles, as shown in Figure 3.5. This is mostly seen in processes where smaller particles are produced and the small solidified powder particles can be drawn back up in the process and stick to the not yet solidified particles [49].

3.2.2 Plasma Atomization

The principle of the process is that the powder is atomized by the introduction of a solid metal wire or a stream of molten metal in the centre of several converging thermal plasma torches [51]. The plasma is generated by introducing an electric discharge into an argon gas. The gas will be partly ionized and heated to a temperature up to 11 000 K, whereas the non-ionized gas

will reach a temperature of 2000-10 000 K [51]. The process is performed in an inert environment to prevent contamination [52].

In the case of titanium, which is rather reactive, the starting material is in the form of a wire. The material is melted and atomized at the same time, which gives a purer material than having a molten bath that reacts with the environment [51].

The plasma torches create a rather large hot zone where the particles have time to form completely spherical particles due to the surface tension force before solidifying [52]. The average diameter of the particles is approximately 45-90 μm [51].

The advantage of plasma atomization is that it gives a spherical powder with few satellites [52]. The drawback of this method is its low productivity and highly refined raw material (wire), which makes plasma atomized powder more expensive than gas atomized powder [42].

3.2.3 Plasma rotating electrode process

Plasma rotating electrode process, PREP, is a centrifugal atomization process where the centrifugal force breaks up the liquid into droplets that are thrown out. The rod electrode is melted at one end by an arc plasma torch while it is rotating [50], see Figure 3.6. The droplets are thrown out and solidify in the inert gas in the container before hitting the walls [53]. Similar to the earlier mentioned plasma atomization process, the fast solidification and the exclusion of a molten bath makes it suitable for highly reactive titanium alloys [50].

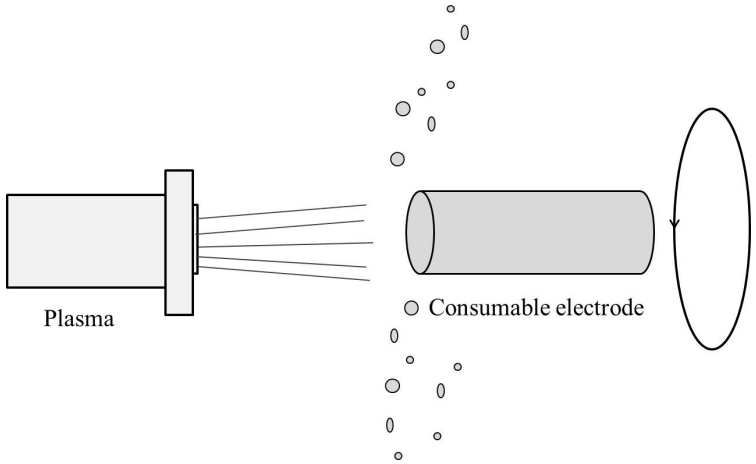

Figure 3.6: Schematic of the principle of plasma rotating electrode process. Adapted from [50].

The powder particles produced by this method have a narrower range of the particle size [50]. The average particles size is normally between 50-400

μm depending on the alloy [49], [50]. The particles have a smooth surface, a high degree of sphericity and the particles are completely solid without any gas-filled particles [50]. Moreover, there are no or very few satellites on the particle surface [54]. The disadvantages are the limitations of the rotating speed, which determines the size of the particles, and the price of the bar as starting material [50].

3.2.4 Plasma spheroidization

Another way of producing spherical powder is by using non-spherical, angular or flaky powder particles as starting material; these are first produced by mechanical methods, such as crushing [55]. Such powder particles are heated and melted in a plasma jet while falling down and form spheres before solidifying due to the surface tension [56]. In addition to making the powder spherical, this treatment may remove pores; impurities may also be evaporated by the heat [55]. However, the drawback is that two different methods are needed.

Chapter 4

Material and methods

In this chapter, the first section gives information about powder samples that were examined in this project. This is followed by the theoretical background of the methods used and the experimental procedures.

4.1 Powder samples

All Ti-6Al-4V powders used in this project were provided by Arcam. The powders have a diameter in the range of 45 to 105 μm, and follow the standard specification of the chemical composition listed in Table 4.1. The powder samples are produced by three different manufacturers, in this report referred to as A, B and C.

Table 4.1: Chemical composition, ASTM F2924 Standard specification for additive manufacturing Ti-6Al-4V with powder bed fusion [22]

Element	Composition, wt%	Composition, at%
Al	5.5-6.75	9.2-11.3
V	3.5-4.5	3.1-4.0
Fe	<0.3	<0.2
O	<0.2	<0.6
C	<0.1	<0.4
N	<0.05	<0.2
H	<0.015	<0.7
Other elements, each	<0.1	-
Other elements, total	<0.4	-
Ti	Balance	Balance

When using the powders in the EBM process, Arcam has detected that the powders from different manufacturers behave differently; for example, more pre-heating is needed to avoid the charging of the powder particles in

some cases. Furthermore, it has also been detected that the powders behave differently when new and when it has been recycled in the process.

The aim of the study is to compare the surface chemistry, the oxide thickness and morphology of powders from different manufacturers and to determine how the recycling in the EBM process and the anti-satellite treatment affect the surface oxide.

Table 4.2: Powder samples investigated in this study

Name	Manufacturer	Batch	Condition
A1-new	A	1	New
A2-new	A	2	New
A2-rec	A	2	Recycled once
A3-before	A	3	Before anti-satellite treatment
A3-after	A	3	After anti-satellite treatment
B1-new	B	1	New
B1-rec	B	1	Recycled several times
C1-new	C	1	New
C2-rec	C	2	Recycled
C3-rec	C	3	Recycled

In Table 4.2, all the powder samples investigated in this study are listed. The powders called 'new' were as-received and not prepared in any way. The recycled powders have been run in the EBM process for several cycles and consist of powder particles from different conditions. For example, there are particles that have been affected by the beam in every cycle and particles that have never been affected. However, the sample A2-rec has only been recycled once. In this case, the powder is taken from semi-sintered agglomerated powder that has been exposed to the electron beam.

In order to reduce the amount of satellites on the powder particles, Arcam has evaluated a non-disclosed treatment. Powder A3 has been examined both before and after this anti-satellite treatment to investigate if it has any effect on the surface oxide or the morphology of the powder.

The chemical compositions of all samples are listed in Table 4.3. For some of the samples tested in different conditions, only the oxygen content is measured. However, the content of the metallic elements can be assumed to be the same for both samples, based on experiences from Arcam.

Table 4.3: Chemical composition of the powder samples in wt%

Element	A1-new	A2-new	A2-rec	A3-before	A3-after
Al	6.18	6.30	-	-	6.40
V	4.00	4.11	-	-	4.12
Fe	0.18	0.18	-	-	0.20
O	0.130	0.130	0.162	0.084	0.0875
C	0.013	0.110	-	-	0.006
N	0.036	0.005	-	-	0.012
H	0.002	0.003	-	-	0.002
Ti	bal.	bal.	bal.	bal.	bal.
Element	B1-new	B1-rec	C1-new	C2-rec	C3-rec
Al	6.40	-	6.17	6.39	6.24
V	4.06	-	4.08	4.18	4.03
Fe	0.180	-	0.089	0.096	0.053
O	0.110	0.19	0.136	0.145	0.146
C	0.010	-	0.026	0.02	0.063
N	0.010	-	0.006	0.003	0.003
H	0.002	-	0.005	0.004	-
Ti	bal.	bal.	bal.	bal.	bal.

4.2 X-ray Photoelectron Spectroscopy

X-ray photoelectron spectroscopy (XPS), also called Electron Spectroscopy for Chemical Analysis (ESCA), is a technique used for surface characterization of materials to determined the chemical composition, the chemical states and element distribution in depth. XPS is often used to investigate corrosion, surface treatment, metallurgy, surface coatings, electronics etc. [57].

4.2.1 Principle

The sample is irradiated with soft X-rays and the kinetic energies (E_k) of the emitted electrons are measured [58], see Figure 4.1. The most commonly used X-ray sources are AlKα (1486.6 eV) and MgKα (1253.6 eV) [59]. The binding energy (K_B) of the photoelectrons can be calculated using Equation 4.1.

$$E_B = hv - E_K - \phi \tag{4.1}$$

where hv is the energy of the X-ray photon and ϕ is the spectrometer work function [59].

Besides photoelectrons, Auger electrons are also emitted, as shown in Figure 4.1. The photoelectron leaves a hole in an inner shell making an

electron from an outer shell occupy the vacancy [58]. The energy released emits another electron, the Auger electron. The energy difference between the first ion and the double-charged ion equals the kinetic energy of the Auger electron.

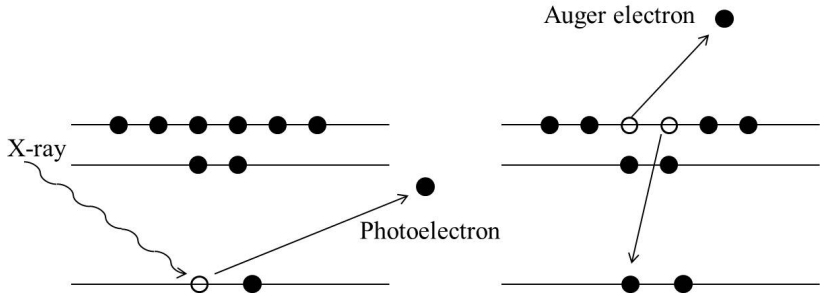

Figure 4.1: Principle of XPS and AES. Adapted from [58].

The binding energy is the energy needed to ionize an atom. It can be considered as the energy difference to the Fermi level, which by its definition equals zero binding energy [58]. All elements except hydrogen can be detected by this method [60].

The inelastic mean free path (IMFP), λ, is the average distance that an electron can travel without inelastic scattering [57]. When only one direction is interesting, the term attenuation length (AL) is used which is dependent of the kinetic energy of the electrons. The X-ray photons can penetrate into a solid material up to a few micrometers whereas the electrons have an attenuation path of a few nanometers in the material without losing energy. This is the reason for the surface sensitivity of the technique.

The notation of the different photoelectron peaks are written in the form nl_j where n is the principal quantum number, l is the angular momentum and j is the total angular momentum; 1s, $2p_{1/2}$, $2p_{3/2}$ are some examples. The angular momentums l=0, 1, 2, 3 correspond to the orbitals s, p, d, f respectively. The total quantum number is j=l+s, where s is the spin quantum number [57]. Doublets are formed due to spin orbit coupling for orbitals higher than the s orbital, such as p, d and f levels. However, the relative intensity of the components of the doublets are constant which is 1:2 for p levels, 2:3 for d levels and 3:4 for f levels, respectively [58].

4.2.2 Instrumentation

An XPS-instrument includes an X-ray source, a sample stage, a lens, an analyzer and a detector [57], as seen in Figure 4.2. The analysis is performed in ultra-high vacuum, about 10^{-8} Pa, to avoid surface contamination [57] and the collision of the electrons with residual molecules [60]. In the X-ray source, there is a hot filament and an anode. The voltage potential between

them releases electrons from the filament and accelerates them towards the anode, which generates X-rays [57]. Monochromators are mostly used for Al anode to increase the energy resolution and to eliminate satellite signals from Kα_3 and Kα_4 X-rays. The analyser measures the kinetic energy of the electrons. The area analysed is approximately 1 mm^2.

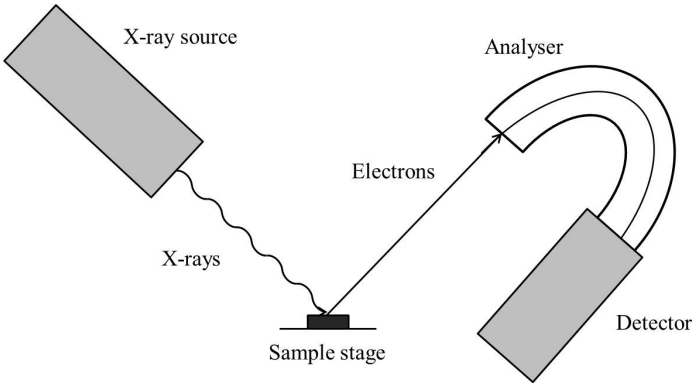

Figure 4.2: Schematic of an XPS instrument. Adapted from [61]

Sample preparation is in general not critical for the XPS-analysis; the sample can often be mounted mechanically and studied in as-received condition [60]. When powder is used, it is often mounted on an adhesive polymeric film, although the film may disturb the vacuum system. Other methods used are supporting the powder on a metallic mesh, pressing the powder into pellets or pressing it into a foil of a soft metal [58]. However, removal of volatile material is necessary in order not to destroy the ultra high vacuum.

4.2.3 Information obtained from XPS-data

For XPS-data, a lot of different information can be obtained. The most important techniques will be described in this section.

Element identification and quantification

The result of an XPS measurement is a spectrum with the binding energies on the x-axis and the intensity, i.e. the discrete number of excited electrons detected, on the y-axis. An example of a wide-scan survey spectra of titanium is shown in Figure 4.3 and a detailed multiplex spectra is shown in Figure 4.4. Each element has a unique set of individual peaks from electrons at different energy levels. The background in the spectra is created by electrons with low kinetic energy that despite that they are undergoing energy loss while colliding with other electrons, are able to leave the surface [58]. In addition to the peaks from the photoelectrons, some peaks from the Auger electrons may be detected in the spectrum.

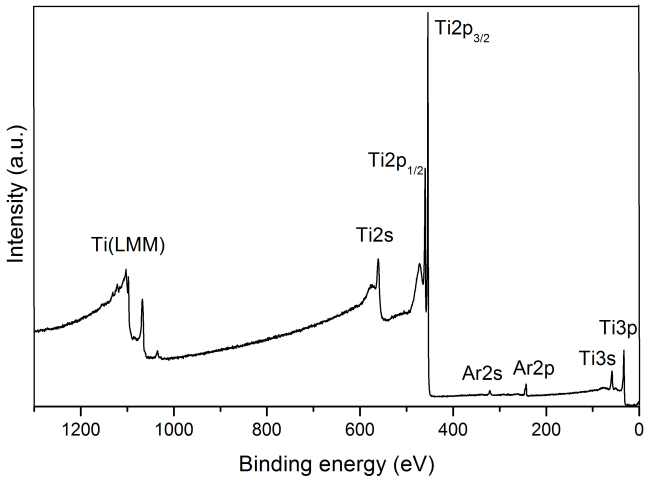

Figure 4.3: An XPS survey spectra for titanium with all the characteristic photoelectron peaks and also the Ti(LMM) peak from Auger electrons. The argon in the spectra comes from the sputtering to obtain a clean sample surface.

The intensities of the peaks (area under the peak), I, may be used to determine the chemical fraction of any element x by using the following equation [58]:

$$C_x = \frac{I_x/S_x}{\sum_i I_i/S_i} \tag{4.2}$$

where S is the sensitivity factor. This factor compensates for the fact that the detector does not have the same ability to detect electrons from different energy levels and elements.

Chemical states

The chemical environment, such as the oxidation state and the compound, affects the binding energy [60]. The difference in binding energy in the XPS spectrum is called the chemical shift. Both initial and final state conribute to the chemical shift. For example, in a positive ion, the lack of electrons results in higher binding energy for the remaining electron, and the opposite effect for negatively charged ions [60]. An example of a chemical shift of titanium can be seen in Figure 4.4, where the ion Ti^{4+} in the oxide TiO_2 has a higher binding energy than the metal. The ability to determine the chemical states is one of the main advantages of this technology [57].

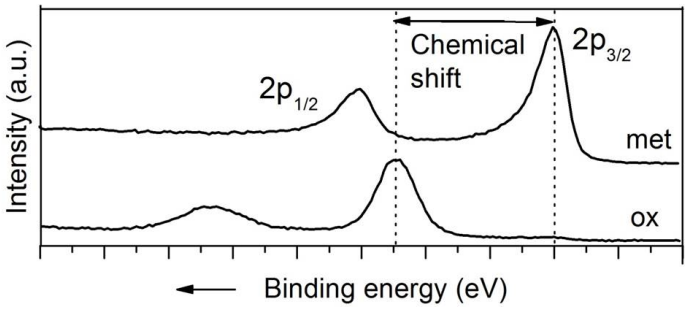

Figure 4.4: Multiplex spectra to show the chemical shift of titanium oxide TiO_2 with respect to metallic state

Depth profile and surface layer thickness

In order to examine the in-depth distribution of elements, two methods are commonly used: a non-destructive method and a destructive method where the material is sputtered away layer by layer.

Generally, if the surface layer is thinner than three times the attenuation length, the element distribution in depth can be studied by changing the take-off angle in order to change the sampling depth [57]. This is called angle resolved XPS (ARXPS). If the oxide is so thin that the metal peak can be detected, the oxide thickness may be calculated from the intensity ratio between the metal and the oxide peak using the following equation [24]:

$$a = \lambda_{Ti}^{ox}(sin\theta \ \ ln(1 + I_{Ti}^{ox}/I_{Ti}^{met} \times I_{Ti}^{ox,\infty}/I_{Ti}^{met,\infty})) \tag{4.3}$$

where a is the oxide thickness (Å), θ is the take-off angle, λ_{Ti}^{ox} is the attenuation length for titanium in the titanium oxide (Å), I_{Ti}^{ox} and I_{Ti}^{met} are the intensities of titanium from the oxide and metal respectively and $I_{Ti}^{ox,\infty}$ and $I_{Ti}^{met,\infty}$ are the intensity values from semi-infinite thick metal and oxide phases respectively. The equation can only be used for the case of $a^{ox} + a^{c} \leq 3\lambda^{ox}$, where a^{c} is the thickness of the surface contamination layer [57].

In the case of a thicker layer, ion sputtering is often used; the surface is then bombarded by Ar^+ or Xn^+ ions to remove the outermost atom layers [57]. By repeated sputtering and XPS analyses, a depth profile of the chemical composition varying with the sputtering time may be obtained. From this graph, the oxide thickness can be estimated as the depth where the oxygen content is reduced to half of its maximum value.

The drawback of this method is that it is destructive and that the ion sputtering affects the surface; some elements are more easily sputtered away than others, and Ar^+ may stick to the surface and also drive surface species into the matrix [60]. If the vacuum system is poor, the surface can be

contaminated in the chamber after sputtering. The ion sputtering can also affect the chemical states as discussed in Section 2.5.1. In short, inert ion bombarding may change both the composition and the chemical state of the surface.

4.2.4 Experimental procedure

The analysis was performed with an XPS-PHI5500 instrument. The X-ray source used was a monochrom AlKα with an energy of 1486.6 eV. The power was 350 W and the voltage 14 kV. The vacuum in the system was approximately 10^{-7} Pa. The emitted area was roughly a square of 0.8×0.8 mm. The standard take-off angle used was 45°.

Ar^+-ion etching was used to sputter away atoms from the surface layer to make a depth-profile. The beam voltage was 4 kV and the raster size 4×5 mm. The sputtering rate calibrated on a Ta_2O_5/Ta foil with a known oxide thickness was 25.5 Å/min.

The survey scan was performed in the binding energy range of 0-1100 eV with a pass energy of 93.5 eV in order to detect the elements present. Afterwards, detailed multiplex scans for the interesting peaks covering O1s, C1s, N1s, Ti2p, Al2p, Al2s, V2p, Cu2p and Y3d were made, with a pass energy of 23.5 eV in order to obtain more detailed information and enable the identification of the chemical states.

In the calculation of the oxide thickness from Equation 4.3, the attenuation length λ_{Ti}^{ox} was set to 17 Å [24]. The intensity values $I_{Ti}^{ox,\infty}$ and $I_{Ti}^{met,\infty}$ were taken from reference specimens.

Mounting methods

Three different ways of mounting the powder in the XPS were examined: a tape, silver paint and by pressing it onto a pure copper plate.

The tape was a double-sided adhesive and conductive carbon tape from Agar Scientific [62]. To mount it, the powder was placed on aluminium foil and one side of a piece of tape was pressed onto the powder. An Agar silver paste was used for the second mounting method. It consists of fine flake silver suspended in methyl iso-butylketone ($((CH_3)_2CHCH_2C(O)CH_3$) [63]. A thin layer of silver paste was placed on a metal piece, which was dipped in the powder and then was left to dry over night to evaporate the solvent. In the third method, a soft pure copper plate was cut into pieces of adequate size, then ground and finally ultrasonically cleaned in ethanol. The powder was then lightly pressed on the copper plate. For all methods, the samples were finally blown with nitrogen gas or compressed air to remove loose particles from the surface and then mounted mechanically on the sample holder for the XPS analysis.

Analysis of spectra

The XPS spectra were analysed using the software programs PC Access ESCA V7.2C, Physical Electronics, and Multipak. The intensities of the peaks (areas) were determined by means of PC Access ESCA V7.2C, Physical Electronics software. When the powder was mounted on copper, the Cu3s peak overlapped with Al2s and Cu3p overlapped with the Al2p. Therefore, to obtain the intensity (area) of aluminium, curve fitting in Multipak was done using the Gaussian Lorentz function. A pure copper plate was analysed to get a good reference peak. By curve fitting and examination of the chemical shift, the chemical states were also determined.

4.3 Scanning Electron Microscopy

A scanning electron microscope (SEM) is used for making high resolution and depth-of-field images and for chemical analyses of small areas [64].

4.3.1 Principle and instrumentation

An SEM microscope consists of an electron gun, an electron optical system and an electron detection system [65]. The system is under vacuum to avoid the electrons to scatter with the gas molecules [64]. The electrons have an energy of 1 to 30 keV; the electron lens system focuses the beam to a diameter of 1 to 10 nm [65]. The beam scans over the sample surface and emits electrons that penetrate into the specimen surface, interact with it and generate secondary electrons and backscattered electrons. The secondary electrons are generated by inelastic collisions leading to emission of electrons close to the surface. Theses electrons give topographical contrast and a high resolution image. The backscattered electrons are electrons from the beam that are elastically scattered from deeper down in the material. The atomic number contrast is higher for the backscattered electrons than the secondary electrons, which enables the detection of different phases and grain boundaries [64].

4.3.2 Experimental procedure

The SEM analysis was performed in an DSM 940 A instrument. The powder was glued onto the aluminium stub with silver paint and all loose powder particles were gently removed with pressured air. The vacuum in the sample chamber was between 10^{-4} and 10^{-5} Pa and an acceleration voltage of 20 kV was used.

Chapter 5

Results

Firstly, the results of the different mounting methods for the XPS analysis are presented leading to a selection of mounting method of the powder for the XPS-analysis in the project. Secondly, the results of all samples from the XPS and SEM analyses are reported. The powders from different manufacturers are compared and this is followed by a description of the effects of the recycling of the powder and the anti-satellite treatment.

5.1 Selection of mounting method of the powder for the XPS-analysis

When different mounting methods were tested, the same powder, A1-new, was used. All tests showed quite a high nitrogen content that afterwards was identified as a nitrogen contamination from the powder production process at the manufacturer [42], and could therefore not be related to the mounting methods.

The XPS-survey spectrum for the different methods are shown in Figure 5.1. The tape and silver paste give high carbon content compared to the copper plate, both before and after sputtering. Furthermore, the tape has some contamination of silicon and the silver paste has traces of chlorine. Therefore, pressing the powder onto a copper plate seemed to be the best method and was used in this project. However, the drawback is that the powder particles may be deformed during the pressing as shown in the SEM pictures in Figure 5.2. Cavities in the copper plate can also be seen at the locations where particles have been pressed onto the plate without sticking. Another drawback is that curve fitting is needed for a quantitative analysis due to the overlapping of the core level XPS peaks of copper and aluminium.

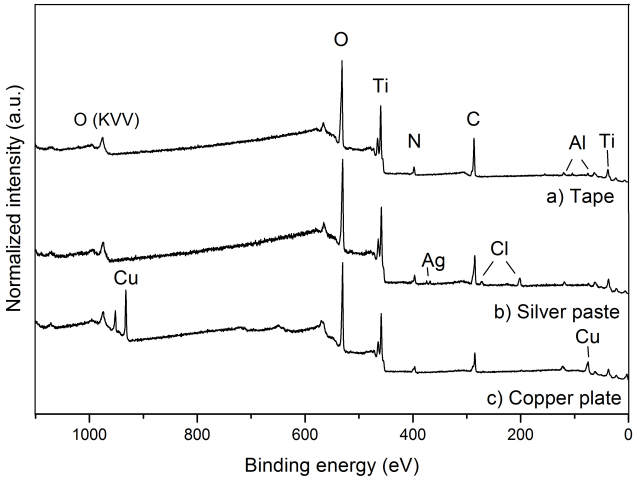

Figure 5.1: XPS survey spectra for the powder A1-new mounted in three different ways: a) double adhesive tape, b) silver paint or c) pressed onto a copper plate.

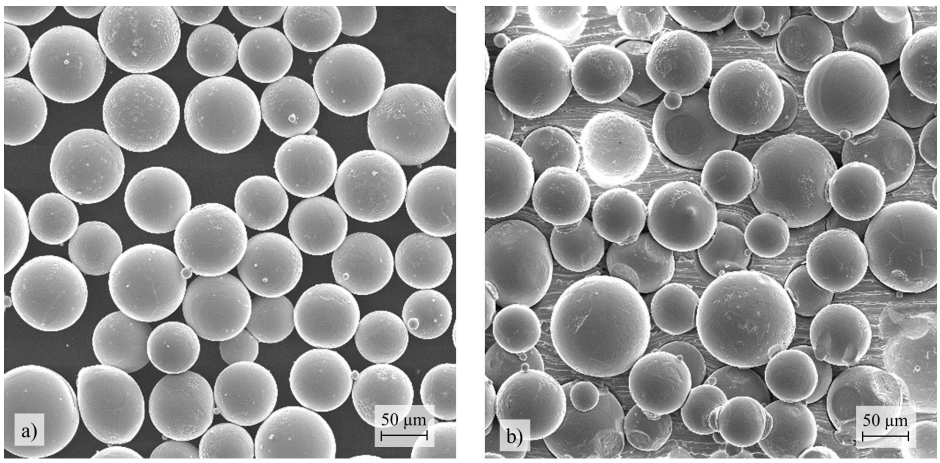

Figure 5.2: Powder B1-new mounted on a) tape and b) pressed onto a copper plate.

5.2 Comparison of powders from different manufacturers

This section deals will the differences between the powders from different manufacturers. The chemical composition, the depth profiling, the chemical states and the oxide thickness obtained from XPS information, as well as the SEM pictures, are included.

5.2.1 Identification, quantification and depth profiling by XPS

The elements detected on all powder surfaces were oxygen, carbon, nitrogen, titanium, aluminium and vanadium. The iron content in the samples was too low to give a detectable peak in the spectra. On the samples from manufacturer B, a trace of chlorine contamination was found on the surface, but it was eliminated after sputtering. On all three powders from manufacturer C, yttrium was also found on the surface. The XPS survey spectra of the three samples C1-new, B1-new and A2-new, are shown in Figure 5.3, where all elements are labelled except vanadium because of the low intensity of its the peak.

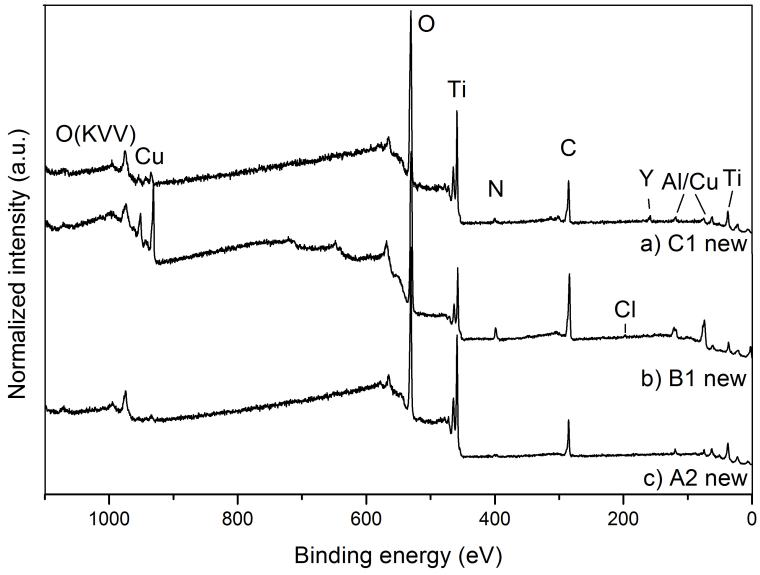

Figure 5.3: XPS survey spectra of the three samples, a) C1-new, b) B1-new and c) A2-new, showing the elements detected at the surface.

The difference in the level of the background on the left side in Figure 5.3 is due to the coverage of powder on the copper plate. With poor coverage of

the powder, more electrons from the copper are detected giving a stronger peak in the spectra and consequently also more inelastic scattered electrons, which contribute to the raised background, as showed in the spectrum from B1-new.

In Figure 5.4, the depth profiles of the new powder samples from all manufacturers can be compared. The surfaces were contaminated by carbon, as there is a large decrease of carbon after the first sputtering. Very small amounts of vanadium were observedont the top surfaces, but the content is somewhat higher for powder C. In both types of depth profiles, the vanadium content is lower on the outermost surface and is increasing with the sputtering time.

The cation graphs in Figure 5.4 show only the metallic elements, in order to focus on the variations of the elements in the alloy without the oxide and the contaminations. In the depth profiles in Figure 5.4 , the powder samples A2-new and C1-new seem to have a slightly lower aluminium content on the surface than in the bulk. However, when only the metallic elements in the cation profiles are studied, a small enrichment of aluminium on the surface can be detected. For powder B, the enrichment is even higher.

In sample C, a small amount of yttrium was detected on the surface; however it decreases down to zero after sputtering. This might be an indication that the yttrium comes from the processing of the powder. Overlapping of Y3s with N1s peak may lead to a small overestimation of the nitrogen in the depth profile for powder C.

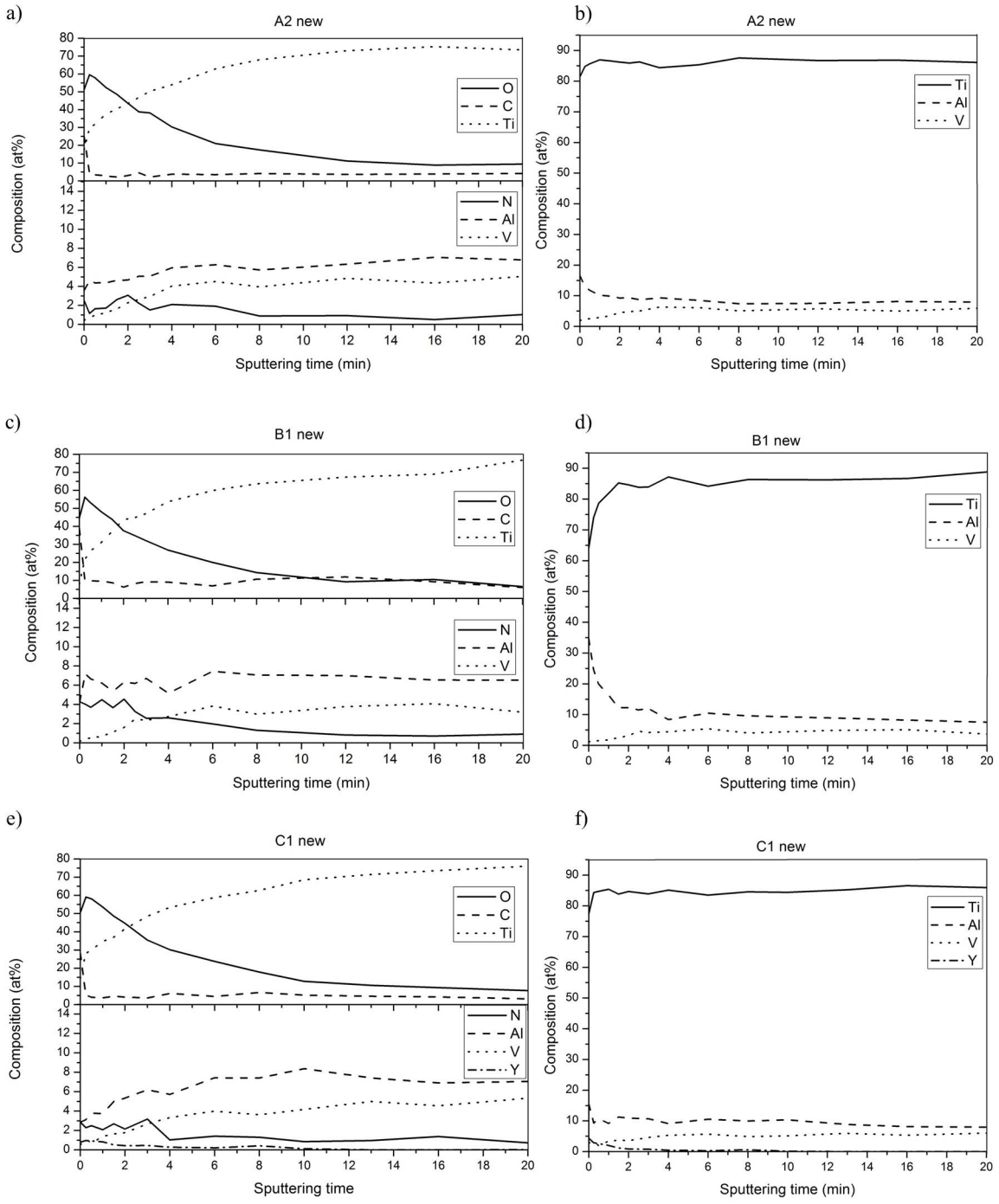

Figure 5.4: XPS depth profiles for A2-new a) and b), B1-new c) and d), and C1-new e) and f). Among these, b), d) and f) are cation profiles that only show the chemical compositions of the metallic elements.

5.2.2 Yttrium contamination

When yttrium had been discovered in the samples from manufacturer C, an additional chemical analysis was made on all powder samples to investigate if traces of yttrium could be detected also in other samples and to obtain the total yttrium content in the bulk. Table 5.1 shows that for all samples from manufacturer A and B, the yttrium content was below the detectable limit and that all samples from manufacturer C have a relatively high yttrium content.

Table 5.1: Average chemical composition of yttrium of the whole powder

Sample	Yttrium wt%
A1-new	<0.001
A2-new	<0.001
A2-rec	<0.001
A3-before	<0.001
A3-after	<0.001
B1-new	<0.001
B1-rec	<0.001
C1-new	0.005
C2-rec	0.005
C3-rec	0.015

5.2.3 Estimation of oxide thickness from XPS data

The thickness of the oxide layers were estimated in two different ways and the results are listed in Table 5.2. In method 1, the thickness was calculated from the depth when the oxygen content has decreased to half of its maximum value in the depth profile.

In method 2, the thickness was calculated from Equation 4.3, using the area ratio between the titanium metal and the oxide XPS peaks. Although the two methods give significantly different values, the ratios between them are almost constant. It is thus concluded that the values cannot be used as absolute results, but a comparison may be made between different samples and different treatments within one method.

Figure 5.5 shows how the oxide thickness, calculated from method 2, varies with the oxygen content. No clear connection can be seen that a higher oxygen content gives a thicker oxide. This may be an indication that the oxygen not only form a thicker oxide, but that the oxygen also diffuses further into the particles.

Table 5.2: Oxide thicknesses (Å)

Sample	Method 1	Method 2	Ratio
A1-new	61.2	34.6	0.57
A2-new	104.6	40.3	0.39
A2-rec	102.0	40.0	0.39
A3-before	79.1	35.3	0.45
A3-after	89.3	40.5	0.45
B1-new	96.6	37.3	0.39
B1-rec	112.2	43.5	0.39
C1-new	107.1	43.0	0.40
C2-rec	117.3	45.9	0.39

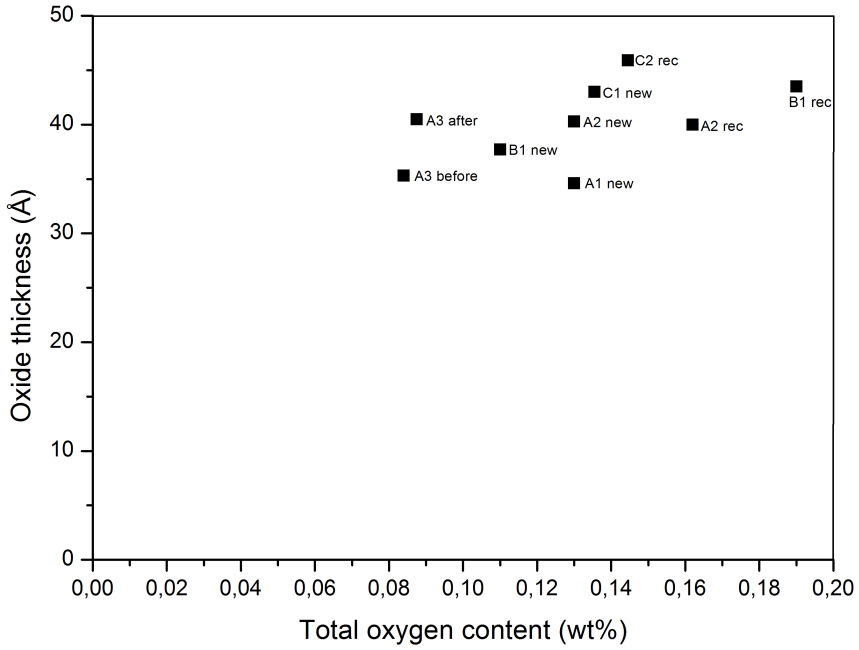

Figure 5.5: Relation between the oxide thickness, calculated from method 2, and the total oxygen content.

5.2.4 Chemical state information

The chemical states of the elements were determined by investigating the binding energy positions and the shapes of the XPS peaks. Because of the effect of sputtering on the chemical states, as discussed in Section 2.5.1, they were only investigated on unsputtered surfaces. The elements investigated were titanium, aluminium, vanadium and nitrogen. No clear differences of the chemical states between the powder samples and different treatments could be detected for these elements. There are small variations of the shapes depending on the difference in ratio between the states.

In Figure 5.6, the titanium 2p peaks are shown for three of the samples. The titanium seems to be mainly in the oxidation state T^{4+}, TiO_2, at a binding energy of 458.7 eV, for all of the samples. Depending on the thickness of the oxide layer, a small peak representing titanium metal at 254.1 eV, can also be detected, as shown most clearly in the case of B1-new in Figure 5.6.

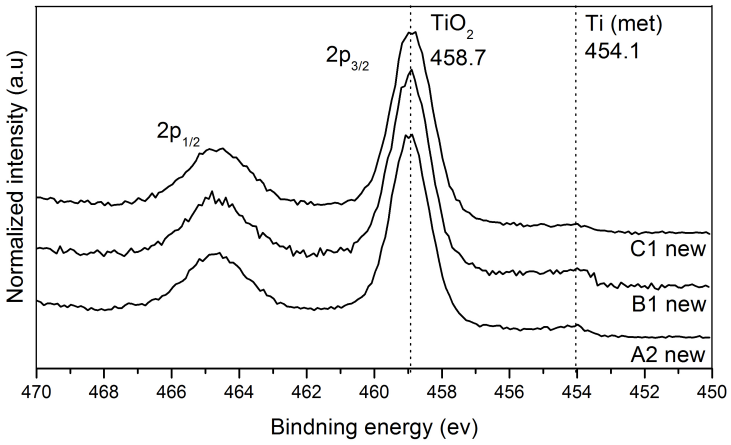

Figure 5.6: XPS peaks for titanium 2p, showing that no differences in chemical states can be seen between the powder samples.

Sample A1-new, which is known to have a significant higher amount of nitrogen, shows, compared to other samples, a very strong peak at around 396.8 eV, representing TiN [66], see Figure 5.7. In this figure, there are also peaks at higher energy, around 400 eV. These peaks disappeared after sputtering and may therefore be identified as organic contamination. The strong TiN peak in the A1-new sample still remained strong after 20 minutes of sputtering.

The aluminium peak overlaps with the copper peak in the XPS spectra. Figure 5.8 shows two examples of the Al2s peaks with varied copper intensity.

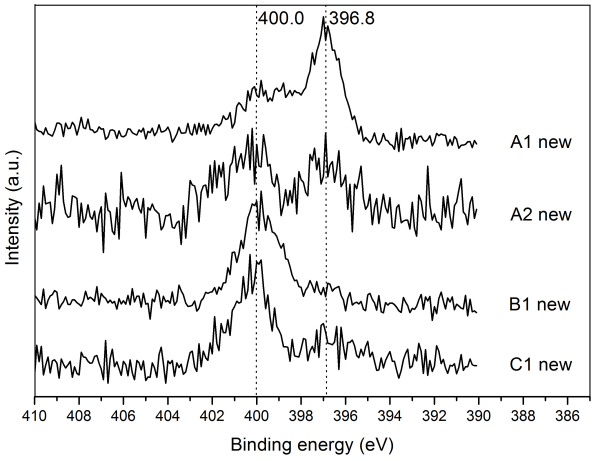

Figure 5.7: N1s XPS photoelectron peaks for four different samples.

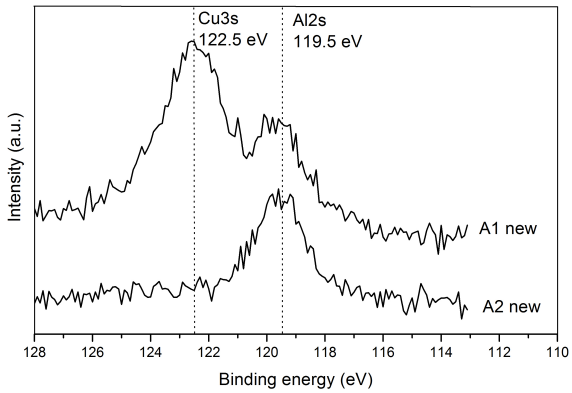

Figure 5.8: XPS peaks of Cu3s overlapping with Al2s for A1-new and A2-new.

Sample A1 has low coverage of powder and a strong signal from copper, whereas powder A2 covers the copper plates so well that almost no copper is detected. The copper reference value is from my own measurements. The aluminium is mostly in Al_2O_3 at a binding energy of 119.5 [67]; no traces of metallic aluminium at lower energies can be seen in the samples.

Vanadium is mainly in V^{5+}, V_2O_5, at the binding energy 516.5 eV [68], as seen in Figure 5.9. Some other oxides might also be present, but they cannot be distinguished particulary due to the low vanadium content and the weak peak.

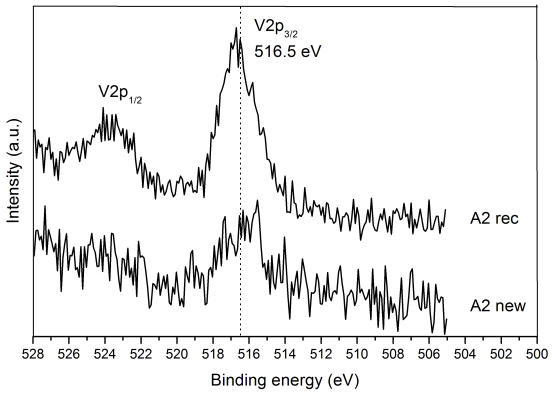

Figure 5.9: Vanadium 2p peaks for new and recycled powder B1.

5.2.5 Shape and morphology of the powder particles

The powder samples were studied in SEM to investigate the shape and morphology of the particles. In Figure 5.10, pictures of the powders particles from all manufactures are shown at different magnifications.

The powder particles in powder B have very few satellites and very high sphericity, whereas both powder A and C have more satellites, rougher surface and more dented and elongated particles. From the pictures it also seems that powder C contains more small particles than the other powders.

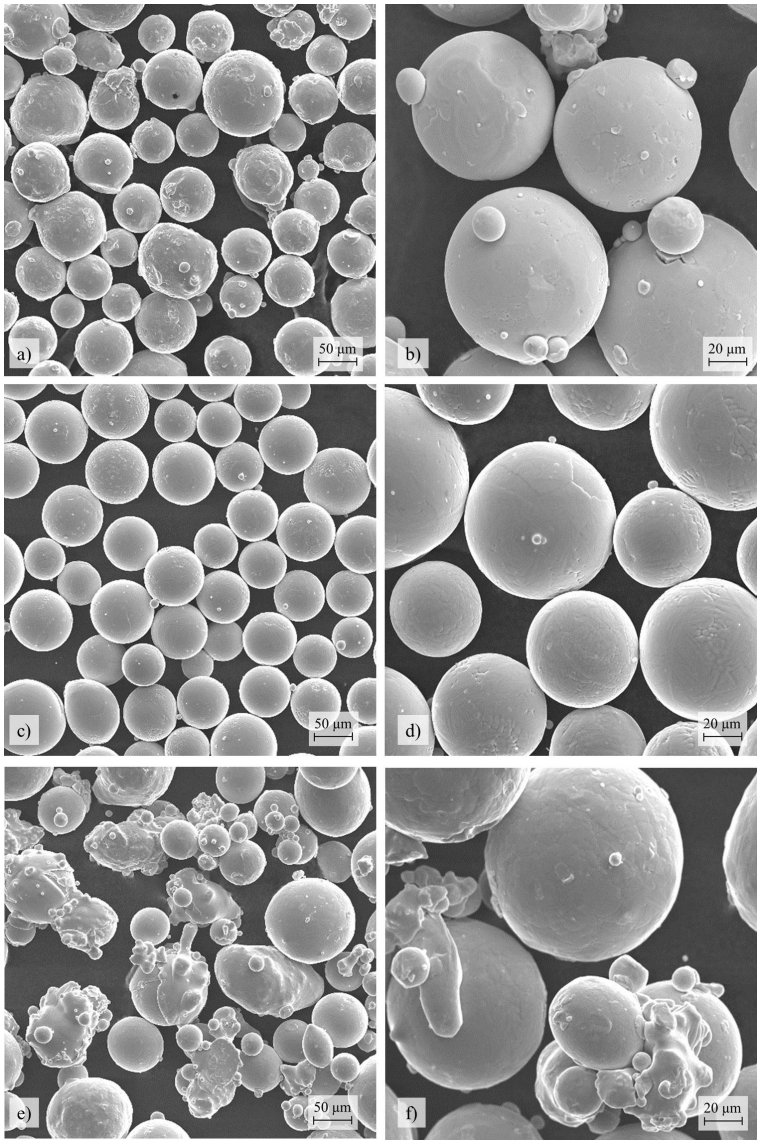

Figure 5.10: SEM pictures of new powders from all manufacturers in different magnifications. a) and b) are from manufacturer A, c) and d) are from manufacturer B, e) and f) are from manufacturer C.

5.3 Effect of recycling of the powder

As seen in both Figure 5.9 and 5.11, the content of vanadium at the outermost surface increases after recycling. In powder B1, the content is almost zero for the new powder and over 1 at% after recycling. In A2, which has only been recycled once, the content of vanadium increases from 0.5 to 2.5 at%. Apart from this, there are no large differences between the chemical composition of powder A before and after recycling.

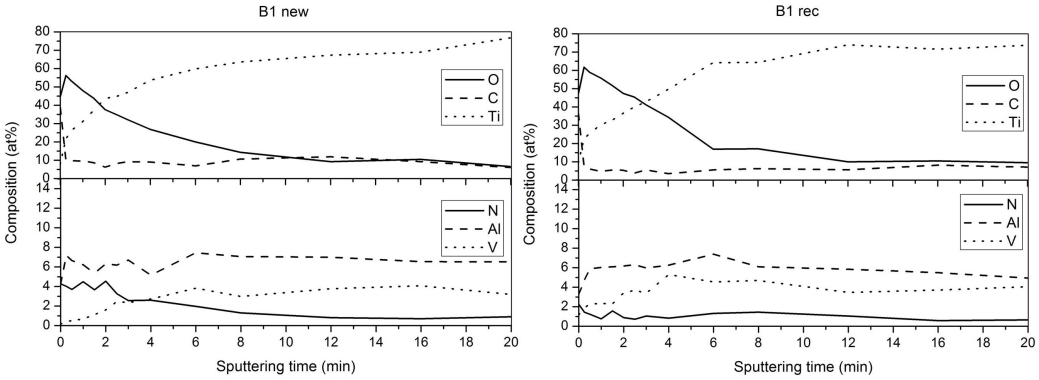

Figure 5.11: Depth profile of powder B1, new and after recycling.

The oxygen content is higher in the depth profile for powder B1 after recycling. Table 5.2 also indicates that the oxide is thicker after it has been recycled. In the A2 powder, the oxides have approximately the same thickness for the recycled as for the new powder. The reason is probably because the powder has only been recycled once, whereas B1 has been recycled several times.

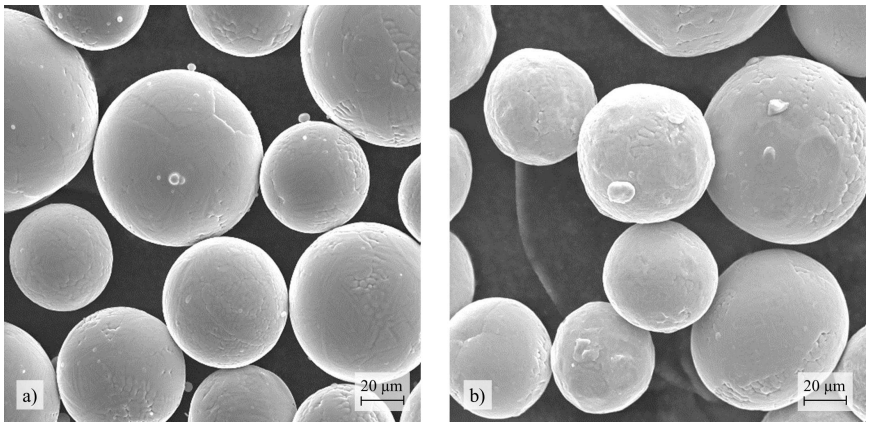

Figure 5.12: Powder B1, a) new and b) after recycling where some deformations and roughness can be seen on the surfaces.

Small deformations are observed on the surfaces after recycling and the surface is also rougher. Figure 5.12 compares the surface morphology between new and recycled particles by SEM. This may be due to the blasting of the powder when the agglomerated powder is removed from the component before it is reused in the process.

5.4 Effect of anti-satellite treatment

Powder sample A3 was examined both before and after an anti-satellite treatment. Figure 5.13 shows the XPS survey spectra of the powders; no differences can be seen in terms of the elements present and the chemical states of the elements.

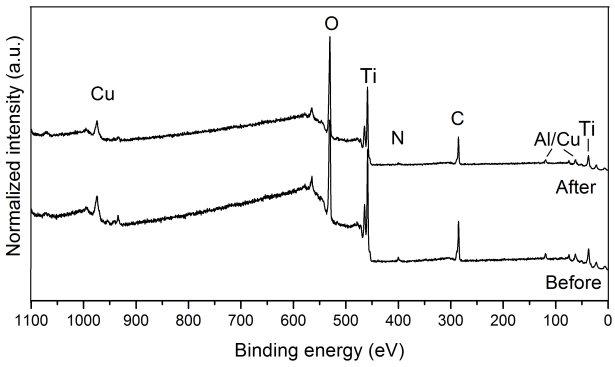

Figure 5.13: XPS survey spectra of powder A3 before and after an anti-satellite treatment.

In the depth profiles of the two samples in Figure 5.14, there are neither any large differences. Figure 5.15 shows the surface morphology of the particles before and after treatment. The amount of satellites and small particles is lower after the treatment, as expected.

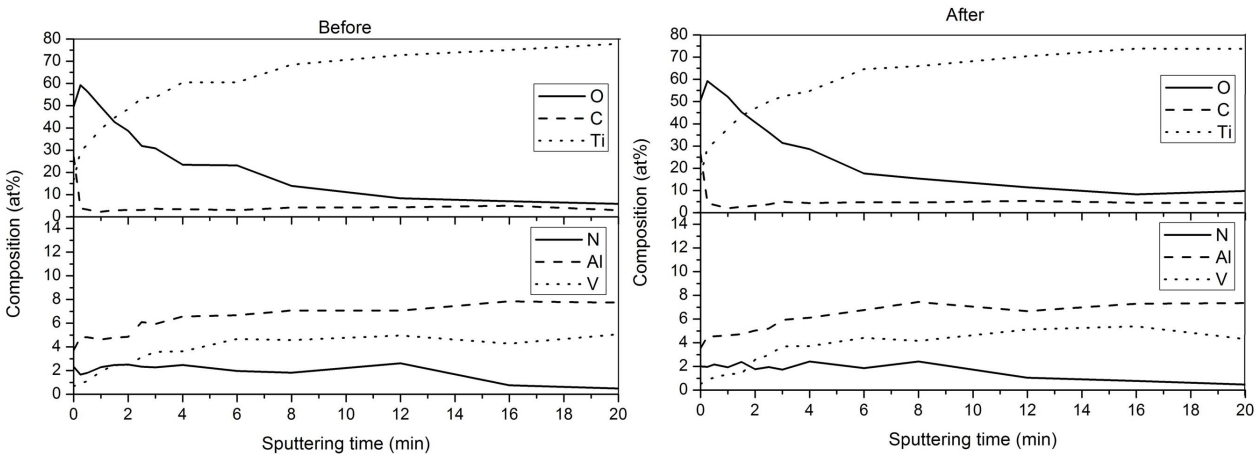

Figure 5.14: Depth profiles for A3 before and after anti-satellite treatment

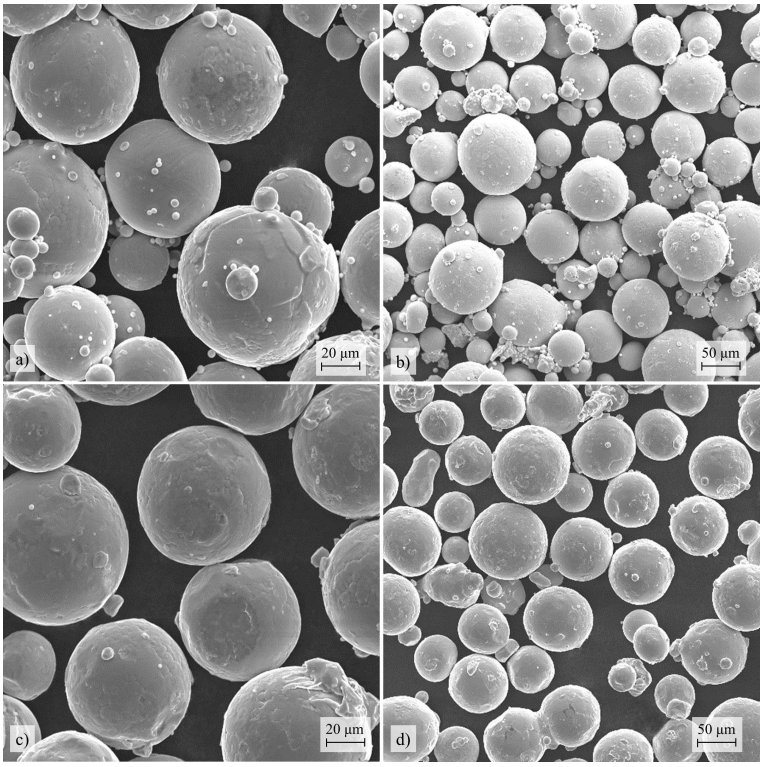

Figure 5.15: Surface morphology of powder A3 in different magnifications, a) and b) before and c) and d) after anti-satellite treatment.

Chapter 6

Discussion

In this project, when different powders are compared, the similarities and differences between them are more important than the absolute thickness of the oxide or the exact chemical composition in the depth profile.

The results are generally consistent with previous studies, in terms of oxide thickness, distribution and chemical states of the alloying elements. The oxide thickness is about 5-10 nm and the titanium and aluminium are found mainly as Ti^{4+} and Al^{3+} in the oxide.

The recycled powder B includes powder particles that have been exposed differently to the electron beam. The oxide thicknesses obtained for the recycled powders are a mean value for all the particles. Hence, for one single recycled particle, the oxide may be thicker than the values listed in Table 5.2. The fact that the oxygen content increases in the recycling limits how many times the powder can be recycled before the allowed oxygen content is exceeded. In practise, this is often solved by blending the powder with a smaller amount of new powder with lower oxygen content after each run.

The ratio of the oxide thicknesses calculated in two different ways was quite constant for the samples. However, the ratio for the powder A1 new was the one that differed the most. The thickness calculated from method 1, using the oxygen content in the depth profile, seems to be low in comparison with the other samples. This might be due to the higher nitrogen content, which affects the oxygen signal in the XPS analysis, which in this powder is lower than for the other samples. However, the nitrogen contamination does not affect the area ratio between the metallic and oxide contribution in the titanium peak, which is used for the calculation with method 2. Therefore, this thickness fits better with the other results. Because of the higher nitrogen content, powder A1 was not used in the comparison between the new powders.

The yttrium in the powders from manufacturer C was just found on the outermost surface, which might be an indications that it comes from contamination during the production. Yttrium is often used for coating crucibles

and molds for molten materials such as titanium, uranium and chromium and their alloys, which are very reactive [69]. This is because yttrium has the highest affinity for oxygen of all elements [70] and the yttrium oxide is very stable even at high temperatures, which makes it resistant to chemical attacks [69]. Some powder standards such as ASTM F1472 in Table 2.2 include a maximum content of yttrium, which is an indication that yttrium has been detected in Ti-6Al-4V powders earlier and that it may have caused problems.

6.1 Experimental uncertainty

The XPS-analysis has been done on spherical particles and not on a flat surface. This gives varied incident angles at different sites of the particles. Because of the spherical particles, the ARXPS was not used to study the depth distribution of the elements in the oxide or the oxide thickness.

The effects of the ion sputtering on the sample surface has to be considered. Firstly, the atoms of some elements may be sputtered away more easily than others; secondly, it is difficult to sputter the surface equally due to "shadow" effects, and thirdly, some atoms may be pushed into the matrix instead of being sputtered away. These effects might lead to some elements on the outermost surface being present in a deeper location in the depth-profile.

The coverage of the titanium powder on the copper plate varied among the samples tested. This could be tracked to the pressing onto the copper plate, which might be improved, but could also depend on the properties of the powder particles. This might affect the accuracy of the compositions in the depth profiles.

Due to the fact the titanium is a very reactive material and despite the ultra high vacuum, contamination on the samples surface inside the chamber has been detected. This may lead to an overestimation of the surface contaminations of oxygen, carbon and nitrogen in the depth-profile if the sample has been contaminated after sputtering.

6.2 Future work

This project has just been a primary study of the powder surfaces to examine if there exist differences originated from powder production and recycling. Further work, including tests in the EBM process, is needed to relate the differences discovered in this report to the different powder production processes and also to their behaviour in the EBM process.

How yttrium in the surface oxide affects the EBM behaviour is in particular of great interest. Moreover, the cause of the yttrium contamination needs to be tracked. Furthermore, it would be interesting to study the form

of the yttrium on the surface. The question is if there are small yttrium oxide particulates attached to the surface or if the yttrium is distributed within the surface oxide.

Some other suggestions of future analysis could be as follows: i) investigation of the phases with X-ray diffraction (XRD), ii) lateral and in-depth distribution of elements both for large and small particles by Auger electron spectroscopy, and iii) chemical analysis with Energy-dispersive X-ray spectroscopy, EDX, to detect lateral variations of the elements.

Chapter 7

Conclusion

- Pressing the powder lightly onto a copper plate was evaluated as the best mounting method for this project.
- The chemical states of the elements in the surface oxide of the powders are the same for all powders. The titanium was mostly in the state of TiO_2 and the aluminium as Al_2O_3.
- No obvious differences on oxide thickness have been observed for new powders from different manufacturers.
- Yttrium was found on the surfaces from all powders from manufacturer C, but not on the surfaces of other powders.
- The vanadium content was impoverished on the powder surface whereas the aluminium content was enriched. The enrichment was higher in sample B.
- The recycled powders show somewhat higher vanadium content on the outermost surface. The particles have small deformations on the surfaces. After recycling several times, the surface oxide was thicker.
- There are no significant differences in the chemical composition or oxide thickness after the anti-satellite treatment.

Bibliography

[1] Donachie, M.J. Jr. *Titanium: A technical guide*. ASM International, USA, 1988.

[2] Lütjering, G., Williams, J.C., and Gysler, A. *Microstructure and properties of materials*, volume 2, chapter 1 Microstructure and mechanical pro-perties of titanium alloys. World Scientific Publishing, Singapore, 2000.

[3] Destefani, J.D. *ASM Handbook*, volume 2, chapter Introduction to titanium and titanium alloys, pages 586–591. ASM International, Ohio, 1990.

[4] Ask, M., Lausmaa, J. and Kasemo, B. Preparation and surface spectroscopic characterization of oxide films on Ti6Al4V. *Applied Surface Science*, (35):283–301, 1988-1989.

[5] Peters, M., Hemptenmacher, J., Kumpfert, J. and Leyens, C. *Titanium and titanium alloys*, chapter 1. Structure and properties of titanium and titanium alloys. Wiley, Weinheim, 2003.

[6] Sibum, H. *Titanium and titanium alloys*, chapter 7. Titanium and titanium alloys - from raw material to semi-finished products. Wiley, Weinheim, 2003.

[7] Peters, M. and Leyens, C. *Titanium and titanium alloys*, chapter 8. Fabrication of titanium alloys. Wiley, Weinheim, 2003.

[8] Lampman, S. *ASM Handbook*, volume 2: Properites and selection: Nonferrous alloys and special-purpose materials, chapter Wrought titanium and titanium alloys, pages 592–633. ASM International, Ohio, 1990.

[9] Leyens, C. *Titanium and titanium alloys*, chapter 6. Oxidation and protection of titanium alloys and titanium aluminides. Wiley, 2003.

[10] RMI Titanium. Titanium alloy guide. Technical report, RMI International Metals, 2000.

[11] Breme, J., Eisenbarth, E. and Biehl, V. *Titanium and titanium alloys*, chapter 16. Titanium and its alloys for medical applications. Wiley, Weinheim, 2003.

[12] Gibbons. *ASM Handbook*, volume 23, chapter Introduction of medical implant materials, pages 3–5. ASM International, 2012.

[13] Tengvall, P. and Lundström, I. Physico-chemical considerations of titanium as a biomaterial. *Clinical Materilas*, 9:115–134, 1992.

[14] J.B Park and Y.K. Kim. *Biomaterials*, chapter Metallic biomaterials, pages 1–20. CRC Press, 2002.

[15] Markovsky, P.E. and Semiatin, S.L. Microstructure and mechanical properties of comercially-purity titanium after rapid (induction) heat treatment. *Journal of Materials Processing Technology*, 210:518–528, 2010.

[16] Terlinde, G. and Fischer, G. *Titanium and titanium alloys*, chapter 2. Beta titanium alloys. Wiley, Weinheim, 2003.

[17] Facchini, L., Magalini, E., Robotti, P. and Molinari, A. Microstructure and mechanical properties of Ti-6Al-4V produced by electron beam meling of pre-alloyed powders. *Rapid Prototyping Journal*, 15(3):171–178, 2009.

[18] Ask, M. Surface characterization of oxide films on Ti6Al4V alloy. Preparation and chemical characterization. Master's thesis, University of Gothenburg, 1985.

[19] Lausmaa, J. *Surface oxides on titanium: Preparation, characterization and biomaterial applications*. PhD thesis, Department of Physics, Chalmers University of Technology and University of Göteborg, 1991.

[20] Balazic, M., Kopa, J., Jackson, M.J. and Ahmed, W. Review: titanium and titanium alloy applications in medicine. *International Journal of Nano and Biomaterials*, 1(1):3–34, 2007.

[21] ASTM Standard F136-11. Standard Specification for Wrought Titanium-6Aluminium-4Vanadium ELI (Extra Low Interstitial) Alloy for Surgical Implant Applications. ASTM International, West Conshohocken, PA, DOI: 10.1520/F0136-11, www.astm.org., 2012.

[22] ASTM Standard F2924-12. Standard Specification for Additive Manufacturing Titanium-6Aluminium-4Vanadium with Powder Bed Fusion. ASTM International, West Conshohocken, PA, DOI: 10.1520/F2924-12 , www.astm.org., 2012.

[23] International standard ISO 5832-3. Implans for surgery - Metallic materials - Part 3: Wrought titanium 6-aluminium 4-vanadium alloy. International Organization for Standardization, Geneva, Switzerland, 1996.

[24] Mattsson, H. and Olefjord, I. *ESCA calibration studies of titanium oxides and titanium hydride.* Department of Engineering Metals. Chalmers University of Technology, 1989.

[25] Miller, J.A. *Titanium; a materials survey.* US Government Printing Office, Washington, 1957.

[26] Diebold, U. The surface science of titanium dioxide. *Surface science reports*, (48):53–229, 2003.

[27] Schutz, R.W. *ASM Handbook*, volume 13B, chapter Corrosion of titanium and titanium alloys, page 252–299. ASM International, Ohio, 2005.

[28] Kasemo, B. and Lausmaa, J. Surface science aspects on inorganic biomaterials. *CRC Critical Reviews in Biocompatibility*, 2(4):335–380, 1986.

[29] Lausmaa, J. Surface spectroscopic characterization of titanium implant materials. *Journal of Electron Spectroscopy and Related Phenomena*, (81), 1996.

[30] Sutherland, D.S., Forshaw, P.D, Allen, G.C., Brown, I.T. and Williams, K.R. Surface analysis of titanium implants. *Biomaterials*, 14(12):893–899, 1993.

[31] Hernández de Gatica, N.L., Jones, G.L and Gardella, J.A. Surface characterization of titanium alloys sterilized for biomedical applications. *Applied Surface Science*, (68):107–121, 1993.

[32] Feng, B., Chen, J.Y., Qi, S.K., He, L., Zhao, J.Z. and Zhang, X.D. Characterization of surface oxide films on titanium and bioactivity. *Journal of Materials Science: Materials in medicine*, (13):457–464, 2002.

[33] McCafferty, E. and Wightman, J.P. An X-ray photoelectron spectroscopy sputter profile study of the native air-formed oxide film on titanium. *Applied Surface Science*, (143):92–100, 1999.

[34] Kofstad, P., Andersson, P.B. and Krudtaa, O.J. Oxidation of titanium in the temperature range 800-1200°C. *Journal of the less-common metals*, 3(2):89–97, 1960.

[35] Carley, A.F., Chalker, P.R., Riviere, J.C and Roberts, M.W. The identification and characterization of mixed oxidation states at oxidised titanium surface by analysis of X-ray photoelectron spectra. *Journal of the Chemical Society, Faraday Transactions*, (83):351–370, 1987.

[36] Sodhi, R.N.S., Weninger, A. and Davies, J.E. X-ray photoelectron spectroscopic camparison of sputtered Ti, Ti6Al4V and passivated bulk metal for use in cell culture techniques. *Journal of Vacuum Science & Technology A*, 9(3):1329–1333, May/June 1991.

[37] Sitting, C., Textor, M., Spencer, N.D., Wieland, M. and Vallotton P.H. Surface characterization of implant materials c.p. Ti, Ti-4Al-7Nb and Ti-6Al-4V with different pretreatments. *Journal of Materials Science: Materials in Medicine*, (10):35–46, 1999.

[38] Lee, W.H. and Hyun, C.Y. XPS study of porous dental implats fabricated by electro-discharge-sintering of spherical Ti-6Al-4V powders in vacuum atmosphere. *Applied Surface Science*, (252):4250–4256, 2006.

[39] Idriss, H. and Barteau, M.A. Characterization of TiO_2 surfaces active for novel organic syntheses. *Catalysis Letters*, (26):123–139, 1994.

[40] Gibson, I., Rosen, D.W. and Stucker, B. *Additive manufacturing technologies*. Springer, New York, 2010.

[41] Wohlers, T. Developments in additive manufacturing. *Manufacturing Engineering*, 144(1):54–59, 2010.

[42] Personal communication with Ulf Ackelid at Arcam.

[43] Ackelid, U. and Svensson, M. Additive manufacturing of dense metal parts by electron beam melting. Conference proceedings at Materials Science & Technology, Pittsburg, USA, 25-29 October 2009.

[44] Arcam. EBM Materials. arcam.com/technology/ebm-materials.aspx. [Cited: 7 August 2012].

[45] Arcam. Arcam A2. www.arcam.com/CommonResources/Files/www.arcam.com/Documents/Products/Arcam-A2.pdf. [Cited: 7 August 2012].

[46] Murr, L.E., Gaytan, S.M., Ramirez, D.A., Martinez, E., Hernandez, J., Amato, K.N., Shindo, P.W., Medina, F.R. and Wicker, R.B. Metal fabrication by additive manufacturing using laser and electron beam melting technologies. *Journal of Materials Science & Technology*, 28(1):1–14, 2012.

[47] Koike, M., Matinez, K., Guo, L., Chahine, G., Kovacevic, R. and Okabe, T. Evaluation of titanium alloy fabricated using electron beam melting system for dental applications. *Journal of Materials Processing Technology*, 2011.

[48] Hu, R.H., Yan, C.F. and Lim, J.K. Porous Ti-6Al-4V fabricated by powder sintering and its property evaluation. *Advanced Materials Research*, 396-398:257–260, 2012.

[49] Lawley, A. *Atomization: The production of metal powders.* Metal Powder Industries Federation, Princeton, New Jersey, 1992.

[50] Dunkley, J.J. *ASM Handbook*, volume 7, chapter Atomization, pages 35–52. ASM International, Ohio, 1998.

[51] Plasma atomization gives unique spherical powders. *Metal Powder Report*, 52(11):34–37, November 1997.

[52] Alagheband, A. and Brown, C. Plasma atomization goes commercial. *Metal Powder Report*, 53(11):26–28, November 1998.

[53] Aller, A.J. and Losada, A. Rotating atomization processes of reactive and refractory alloys. *Metal Powder Report*, 45(1):51–55, January 1990.

[54] Miller, S.A. and Roberts, P.R. *ASM Handbook*, volume 7: Powder metal technologies and applications, chapter Rotating electrode process, pages 87–101. ASM International, Ohio, 1998.

[55] Tekna Plasma Systems. Spherical powders. http://www.tekna.com/technology/spherical-powder/, 2009. [Cited: 13 August 2012].

[56] Ananthapadmanabhan, P.V. and Venkatramani, N. *Non-equilibrium processing of materials.* Pergamon, Amsterdam, 1999.

[57] Olefjord, I. *Surface characterization: a users sourcebook*, chapter X-ray photoelectron spectroscopy. Wiley, Weinheim, 1997.

[58] Wagner, C.D., Riggs, W.M., Davis, L.E. and Moulder, J.F. *Handbook of X-Ray Photoelectron Spectroscopy.* Perkin-Elmer Corporation, Eden Prairie, Minnesota, 1979.

[59] Watts, J.F. and Wolstenholme, J. *An introduction to surface analysis by XPS and AES.* Wiley, West Sussex, England, 2003.

[60] Lumsden, J.B. . *ASM Handbook*, volume 10: Materials Characterizations, chapter X-Ray Photoelectron Spectroscopy, pages 568–580. ASM International, Ohio, 1986.

[61] Kolmakov, A., Dikin, D.A., Cote, L.J., Huang, J., Abyaneh, M.K., Amati, M., Gregoratti, L., Günther, S. and Kiskinova, M. Graphene oxide windows for in situ environmental cell photoelectron spectroscopy. *Nature Nanotechnology*, 6:651–657, 2011.

[62] Agar Scientific. Agar scientific - product list. www.agarscientific.com/catalogue/action_catalogue.asp?spx=1&sat=2&saa=11&jumpto=17CT. [Cited: 28 August 2012].

[63] Agar Scientific. Agar scientific - product list. www.agarscientific.com/catalogue/action_catalogue.asp?spx=1&sat=2&saa=11&jumpto=17AS. [Cited: 7 August 2012].

[64] Verhoeven, J.D. *ASM Handbook*, volume 10: Materials Characterizations, chapter Scanning electron microscope, pages 490–515. ASM International, Ohio, 1986.

[65] Khursheed, A. *Scanning Electron Microscope optics and spectrometers*. World Scientific Publishing Co., River Edge, USA, 2010.

[66] Huravlev, J.F., Kuznetsov, M.V. and Gubanov, V.A. XPS analysis of adsorption of oxygen molecules on the surface of Ti and TiN_x films in vacuum. *Journal of Electron Spectroscopy and Related Phenomena*, 38:169–176, 1992.

[67] Lippitz, A., Kemnitz E., Bose, O. and Unger, W.E.S. C1s and Au $4f_{7/2}$ referenced XPS binding energy data obtained with different aluminium oxides, -hydroxides and -fluorides. *Fresenius' Journal of Analytical Chemistry*, 358:175–179, 1997.

[68] Borgmann, D., Hums, E., Hopfengartner, G., Wedler, G., Spitznagel, G.W. and Rademacher, I. XPS studies of oxidic model catalysts: internal standards and oxidation numbers. *Journal of Electron Spectroscopy and Related Phenomena*, 63:91–116, 1993.

[69] ZYP Coatings. Yttrium oxide products. www.zypcoatings.com/Archived/brochures/Catalog-Yttria.pdf. [Cited: 7 augusti 2012].

[70] Metall Rare Earth. Yttrium Oxide, metall & compounds from Metall Rare Earth Limited. www.metall.com.cn/y.htm. [Cited: 7 August 2012].